NASA-CR-197832

PROBABILISTIC MATERIAL STRENGTH DEGRADATION MODEL FOR INCONEL 718 COMPONENTS SUBJECTED TO HIGH TEMPERATURE, HIGH-CYCLE AND LOW-CYCLE MECHANICAL FATIGUE, CREEP AND THERMAL FATIGUE EFFECTS

Prepared by:

Callie C. Bast, M.S.M.E., Research Engineer
Lola Boyce, Ph. D., P. E., Principal Investigator

Final Technical Report
of Project Entitled
Development of Advanced Methodologies
for Probabilistic Constitutive Relationships
of Material Strength Models, Phases 5 and 6

NASA Grant No. NAG 3-867, Supp. 5 and 6

Report Period:
June 1992 to January 1995

Prepared for:

NATIONAL AERONAUTICS AND SPACE ADMINISTRATION
Lewis Research Center
Cleveland, Ohio 44135

The Division of Engineering
The University of Texas at San Antonio
San Antonio, TX 78249
January, 1995

ABSTRACT

This report presents the results of both the fifth and sixth year effort of a research program conducted for NASA-LeRC by The University of Texas at San Antonio (UTSA). The research included on-going development of methodology for a probabilistic material strength degradation model. The probabilistic model, in the form of a postulated randomized multifactor equation, provides for quantification of uncertainty in the lifetime material strength of aerospace propulsion system components subjected to a number of diverse random effects. This model is embodied in the computer program entitled PROMISS, which can include up to eighteen different effects. Presently, the model includes five effects that typically reduce lifetime strength: high temperature, high-cycle mechanical fatigue, low-cycle mechanical fatigue, creep and thermal fatigue. Statistical analysis was conducted on experimental Inconel 718 data obtained from the open literature. This analysis provided regression parameters for use as the model's empirical material constants, thus calibrating the model specifically for Inconel 718. Model calibration was carried out for five variables, namely, high temperature, high-cycle and low-cycle mechanical fatigue, creep and thermal fatigue. Methodology to estimate standard deviations of these material constants for input into the probabilistic material strength model was developed. Using an updated version of PROMISS, entitled PROMISS93, a sensitivity study for the combined effects of high-cycle mechanical fatigue, creep and thermal fatigue was performed. Then using the current version of PROMISS, entitled PROMISS94, a second sensitivity study including the effect of low-cycle mechanical fatigue, as well as, the three previous effects was performed. Results, in the form of cumulative distribution functions, illustrated the sensitivity of lifetime strength to any current value of an effect. In addition, verification studies comparing a combination of high-cycle mechanical fatigue and high temperature effects by model to the combination by experiment were conducted. Thus, for Inconel 718, the basic model assumption of independence between effects was evaluated. Results from this limited verification study strongly supported this assumption.

NOMENCLATURE

A_i	current value of the i^{th} effect
A_{iU}	ultimate value of the i^{th} effect
A_{iO}	reference value of the i^{th} effect
a_i	i^{th} value of the empirical material constant
b	fatigue strength exponent
c	fatigue ductility exponent
E	modulus of elasticity
K'	cyclic strength coefficient
n	number of effect product terms in the model
n'	cyclic strain hardening exponent
N	current value of high-cycle mechanical fatigue cycles
N'	current value of thermal fatigue cycles
N"	current value of low-cycle mechanical fatigue cycles
N_F	number of high-cycle mechanical fatigue cycles to failure
N'_F	number of thermal fatigue cycles to failure
$2N'_F$	number of thermal fatigue reversals to failure
N''_F	number of low-cycle mechanical fatigue cycles to failure
N_U	ultimate value of high-cycle mechanical fatigue cycles
N'_U	ultimate value of thermal fatigue cycles
N''_U	ultimate value of low-cycle mechanical fatigue cycles
N_O	reference value of high-cycle mechanical fatigue cycles
N'_O	reference value of thermal fatigue cycles
N''_O	reference value of low-cycle mechanical fatigue cycles
q	material constant for temperature
r	material constant for low-cycle mechanical fatigue cycles
R^2	coefficient of determination
s	material constant for high-cycle mechanical fatigue cycles
S	current value of material strength
S_O	reference value of material strength
T	current value of temperature
T_U	ultimate value of temperature
T_O	reference value of temperature

NOMENCLATURE (continued)

t	current value of creep time
t_F	number of creep hours to failure
t_U	ultimate value of creep time
t_O	reference value of creep time
u	material constant for thermal fatigue cycles
v	material constant for creep time
$\Delta\varepsilon_e/2$	elastic strain amplitude
$\Delta\varepsilon_P/2$	plastic strain amplitude
$\Delta\varepsilon_T/2$	total strain amplitude
$\Delta\sigma/2$	stress amplitude
ε'_F	fatigue ductility coefficient
μ	mean
σ	standard deviation
σ'_F	fatigue strength coefficient

TABLE OF CONTENTS

TABLE OF CONTENTS (continued)

LIST OF FIGURES

LIST OF FIGURES (continued)

FIGURE PAGE

LIST OF FIGURES (continued)

FIGURE PAGE

LIST OF FIGURES (continued)

FIGURE PAGE

LIST OF TABLES

LIST OF TABLES (continued)

1.0 INTRODUCTION

Probabilistic methods, for quantifying the uncertainties associated with the design and analysis of aerospace propulsion system components, can significantly improve system performance and reliability. The reusability and durability of aerospace components are of prime interest for economical, as well as, safety related reasons. Life cycle costs including initial design costs and field replacement costs of aerospace propulsion system components are driving elements for improving life prediction capability. Accurate prediction of expected service lifetimes is crucial in the final decision of whether or not to proceed with a particular design. Inaccurate lifetime strength predictions can result in either a lack of adequate life or an overly costly design due to inefficient utilization of material.

This work is part of a larger effort to develop a probabilistic approach for lifetime strength prediction methods [4]. This report presents the on-going development of methodology that predicts probabilistic lifetime strength of aerospace materials via computational simulation. A material strength degradation model, in the form of a randomized multifactor equation, is postulated for strength degradation of structural components of aerospace propulsion systems subjected to a number of effects. Some of the typical variables or effects that propulsion system components are subjected to under normal operating conditions include high temperature, fatigue and creep. Methodology to calibrate the model using actual experimental materials data together with regression analysis of that data is also presented. Material data for the superalloy, Inconel 718, were analyzed using the developed methodology.

Sections 2 and 3 summarize the theoretical and computational background for the research. The above-described randomized multifactor equation is embodied in the computer program, PROMISS [6]. This program was developed using the NASA Lewis Research Center and the University of Texas System Cray-Y-MP supercomputers. Section 4 discusses the strength degradation model developed for high temperature, high-cycle mechanical fatigue, low-cycle mechanical fatigue, creep and thermal fatigue effects, individually. Initial estimates for ultimate and reference values are determined using available data for Inconel 718. A transformation to improve model sensitivity is then discussed. Section 5 presents experimental material data for Inconel 718 and displays the data in the form utilized by the multifactor equation embodied in PROMISS. Temperature, high-cycle mechanical fatigue, low-cycle mechanical fatigue, creep and thermal fatigue data for Inconel 718 are presented. Linear regression of the data is performed to provide first estimates of the empirical material constants, a_i, used to calibrate the model. Additional calibration techniques to improve model accuracy are then discussed. In Section 6, methodology for estimating standard deviations of the empirical material constants is developed as a means for dealing with limited data. These estimated values for the standard deviation, rather than expert opinion, may be used with greater confidence in the probabilistic material strength degradation model. Section 7 presents and discusses cases for analysis that resulted from two sensitivity studies. '93 Sensitivity Study examined the combined effects of high-cycle mechanical fatigue, creep and thermal fatigue at elevated temperatures, while '94 Sensitivity Study included four effects - low-cycle mechanical fatigue along with the three previous effects. Results, in the form of cumulative distribution functions, illustrate the sensitivity of lifetime strength to any current value of an effect. Section 8 presents and discusses model verification studies that were conducted to evaluate the ability of the multifactor equation to model two or more effects simultaneously. Available data allowed for verification studies comparing a combination of high-cycle mechanical fatigue and temperature effects by model to the combination of these two effects by experiment. Methodology and results are reiterated and discussed in Section 9. Conclusions of the current research and recommendations for future research conclude this report. The raw data for all effects, along with material and heat treatment specifications, are provided in the appendix.

2.0 THEORETICAL BACKGROUND

Previously, a general material behavior degradation model for composite materials, subjected to a number of diverse effects or variables, was postulated to predict mechanical and thermal material properties [8,9,13,14]. The resulting multifactor equation summarizes a proposed composite micromechanics theory and has been used to predict material properties for a unidirectional fiber-reinforced lamina based on the corresponding properties of the constituent materials.

More recently, the equation has been modified to predict the lifetime strength of a single constituent material due to "n" diverse effects or variables [4,5,6]. These effects could include variables such as high temperature, creep, high-cycle mechanical fatigue, thermal fatigue, corrosion or even radiation attack. For these variables, strength decreases with an increase in the variable [12]. The general form of the postulated equation is

$$\frac{S}{S_O} = \prod_{i=1}^{n} \left[\frac{A_{iU} - A_i}{A_{iU} - A_{iO}} \right]^{a_i}, \qquad (1)$$

where A_i, A_{iU} and A_{iO} are the current, ultimate and reference values, respectively, of a particular effect; a_i is the value of an empirical material constant for the i^{th} product terms of variables in the model; S and S_O are the current and reference values of material strength. Each term has the property that if the current value equals the ultimate value, the lifetime strength will be zero. Also, if the current value equals the reference value, the term equals one and strength is not affected by that variable. The product form of equation (1) assumes independence between the individual effects. This equation may be viewed as a solution to a separable partial differential equation in the variables with the further limitation or approximation that a single set of separation constants, a_i, can adequately model the material properties.

Calibration of the model is achieved by appropriate curve-fitted least squares linear regression of experimental data [19] plotted in the form of equation (1). For example, data for just one effect could be plotted on log-log paper. A good fit for the data may be obtained by linear regression as shown schematically in Figure 1. Dropping the subscript "i" for a single variable, the postulated equation is obtained by noting the linear relation between log S and

$\log [(A_U - A_O)/(A_U - A)]$, as follows:

$$\log S = -a \log\left[\frac{A_U - A_O}{A_U - A}\right] + \log S_O$$

$$\log \frac{S}{S_O} = -a \log\left[\frac{A_U - A_O}{A_U - A}\right]$$

$$\frac{S}{S_O} = \left[\frac{A_U - A_O}{A_U - A}\right]^{-a} \tag{2a}$$

or,

$$\frac{S}{S_O} = \left[\frac{A_U - A}{A_U - A_O}\right]^{a} . \tag{2b}$$

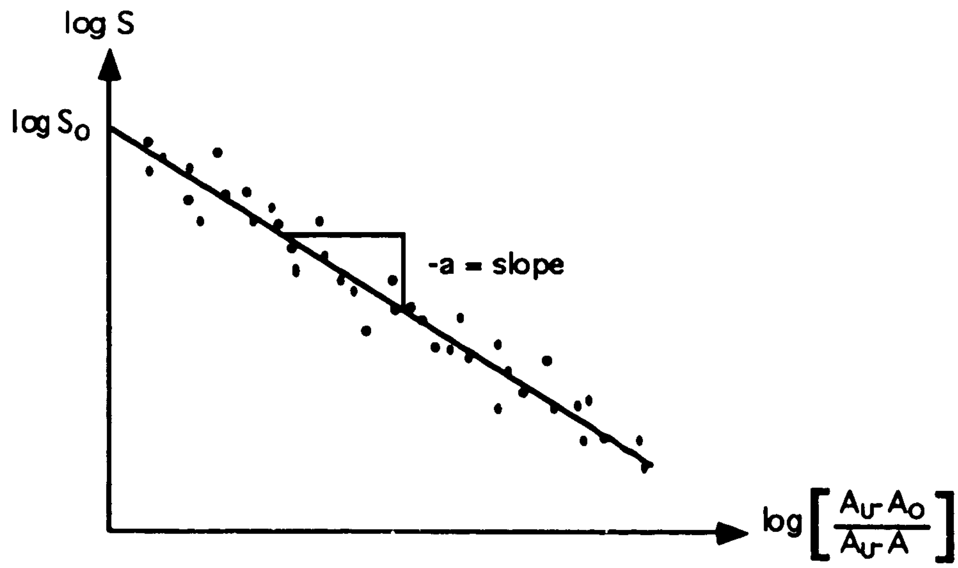

Fig. 1 Schematic of Data Illustrating the Effect of One Variable on Strength.

This general material strength degradation model, given by equation (1), may be used to estimate the lifetime strength, S/S_O, of an aerospace propulsion system component operating under the influence of a number of diverse effects or variables. The probabilistic treatment of this model includes "randomizing" the deterministic multifactor equation through probabilistic analysis by simulation and the generation of probability density function (p.d.f.) estimates for lifetime strength, using the non-parametric method of maximum penalized likelihood [20,22]. Integration of the probability density function yields the cumulative distribution function (c.d.f.) from which probability statements regarding lifetime strength may be made. This probabilistic material strength degradation model, therefore, predicts the random lifetime strength of an aerospace propulsion component subjected to a number of diverse random effects.

The general probabilistic material strength degradation model, given by equation (1), is embodied in the FORTRAN program, PROMISS (Probabilistic Material Strength Simulator) [6]. PROMISS calculates the random lifetime strength of an aerospace propulsion component subjected to as many as eighteen diverse random effects. Results are presented in the form of cumulative distribution functions of lifetime strength, S/S_O.

3.0 PROMISS COMPUTER PROGRAM

PROMISS includes a relatively simple "fixed" model as well as a "flexible" model. The fixed model postulates a probabilistic multifactor equation that considers the variables given in Table 1. The general form of this equation is given by equation (1), wherein there are now n = 7 product terms, one for each effect listed below. Note that since this model has seven terms, each containing four parameters of the effect (A, A_U, A_O and a), there are a total of twenty-eight variables. The flexible model postulates the probabilistic multifactor equation that considers up to as many as n = 18 effects or variables. These variables may be selected to utilize the theory and experimental data currently available for the particular strength degradation mechanisms of interest. The specific effects included in the flexible model are listed in Table 2. To allow for future expansion and customization of the flexible model, six "other" effects have been provided.

Table 1 Variables Available in the "Fixed" Model.

i^{th} Primitive Variable	Primitive Variable Type
1	Stress due to static load
2	Temperature
3	Chemical reaction
4	Stress due to impact
5	Mechanical fatigue
6	Thermal fatigue
7	Creep

Table 2 Variables Available in the "Flexible" Model.

A. Environmental Effects
1. Mechanical
a. Stress
b. Impact
c. Other Mechanical Effect
2. Thermal
a. Temperature Variation
b. Thermal Shock
c. Other Thermal Effect
3. Other Environmental Effects
a. Chemical Reaction
b. Radiation Attack
c. Other Environmental Effect
B. Time-Dependent Effects
1. Mechanical
a. Creep
b. Mechanical Fatigue
c. Other Mech. Time-Dependent Effect
2. Thermal
a. Thermal Aging
b. Thermal Fatigue
c. Other Thermal Time-Dependent Effect
3. Other Time-Dependent Effects
a. Corrosion
b. Seasonal Attack
c. Other Time-Dependent Effect

The considerable scatter of experimental data and the lack of an exact description of the underlying physical processes for the combined mechanisms of fatigue, creep, temperature variations, and so on, make it natural, if not necessary to consider probabilistic models for a strength degradation model. Therefore, the fixed and flexible models corresponding to equation (1) are "randomized", and yield the random lifetime material strength due to a number of diverse random effects. Note that for the fixed model, equation (1) has the following form:

$$S/S_O = f(A_{1U}, A_1, A_{1O}, a_1,..., A_{iU}, A_i, A_{iO}, a_i,..., A_{7U}, A_7, A_{7O}, a_7) \quad (3)$$

where A_i, A_{iU} and A_{iO} are the current, ultimate and reference values of the i^{th} of seven effects as given in Table 1, and a_i is the i^{th} empirical material constant. In general, this expression can be written as,

$$S/S_O = f(X_i), i = 1,..., 28 \quad , \quad (4)$$

where X_i represents the twenty-cight variables in equation (3). Thus, the fixed model is "randomized" and assumes all the variables, X_i, $i = 1,..., 28$, to be random. For the flexible model, equation (1) has a form analogous to equations (3) and (4), except that there are as many as seventy-two random variables. Applying probabilistic analysis [22] to either of these randomized equations yields the distribution of the dependent random variable, lifetime material strength, S/S_O.

Although a number of methods of probabilistic analysis are available, simulation was chosen for PROMISS. Simulation utilizes a theoretical sample generated by numerical techniques for each of the random variables [22]. One value from each sample is substituted into the functional relationship, equation (3), and one realization of lifetime strength, S/S_O, is calculated. This calculation is repeated for each value in the set of samples, yielding a distribution of different values for lifetime strength.

A probability density function (p.d.f.) is generated from these different values of lifetime strength, using a non-parametric method, maximum penalized likelihood. Maximum penalized likelihood generates the p.d.f. estimate using the method of maximum likelihood together with a penalty function to smooth it [20]. Integration of the generated p.d.f. results in the cumulative distribution function (c.d.f.), from which probabilities of lifetime strength can be directly noted.

In summary, PROMISS randomizes the following equation:

$$\frac{S}{S_O} = \prod_{i=1}^{n}\left[\frac{A_{iU} - A_i}{A_{iU} - A_{iO}}\right]^{a_i} . \quad (1)$$

There is a maximum of eighteen possible effects that may be included in the model. For the flexible model option, they may be chosen by the user from those in Table 2. For the fixed model option, the variables of Table 1 are used. Within the product term for each effect, the current, ultimate and reference values, as well as the empirical material constant, may be modeled as either deterministic, normal, lognormal, or Wiebull random variables. Simulation is used to generate a set of realizations for lifetime random strength, S/S_0, from a set of realizations for the random variables of each product term. Maximum penalized likelihood is used to generate the p.d.f. estimate of lifetime strength, from the set of realizations of lifetime strength. Integration of the p.d.f. yields the c.d.f., from which probabilities of lifetime strength can be ascertained. PROMISS also provides information on lifetime strength statistics, such as the mean, variance, standard deviation and coefficient of variation.

4.0 STRENGTH DEGRADATION MODEL FOR INCONEL 718

The probabilistic material strength degradation model, in the form of the multifactor equation given by equation (1), when modified for a single effect, results in equation (5) below.

$$\frac{S}{S_O} = \left[\frac{A_U - A}{A_U - A_O}\right]^{a} = \left[\frac{A_U - A_O}{A_U - A}\right]^{-a} \qquad (5)$$

Appropriate values for the ultimate, A_U, and reference quantities, A_O, had to be estimated as part of the initial calibration of the multifactor equation for Inconel 718. Based on actual Inconel 718 data, these values were selected accordingly for each effect.

4.1 Temperature Model

Equation (5), when modified for the effect of high temperature only, becomes:

$$\frac{S}{S_O} = \left[\frac{T_U - T_O}{T_U - T}\right]^{-q}, \qquad (6a)$$

where T_U is the ultimate or melting temperature of the material, T_O is a reference or room temperature, T is the current temperature of the material, and q is an empirical material constant that represents the slope of a straight line fit of the modeled data on log-log paper. A logical choice for the ultimate temperature value is the average melting temperature (2369 °F) of Inconel 718. Therefore, this value was an initial estimate for the ultimate temperature value, T_U. An estimate of 75 °F or room temperature was used for the reference temperature value, T_O. Substitution of these values into equation (6a) above results in equation (6b) below. Thus, equation (6b) models the effect of high temperature on the lifetime strength of the specified material, Inconel 718.

$$\frac{S}{S_O} = \left[\frac{T_U - T_O}{T_U - T}\right]^{-q} = \left[\frac{2369 - 75}{2369 - T}\right]^{-q} \qquad (6b)$$

4.2 High-Cycle Mechanical Fatigue Model

Equation (5), when modified for the effect of high-cycle mechanical fatigue, becomes:

$$\frac{S}{S_O} = \left[\frac{N_U - N_O}{N_U - N}\right]^{-s} , \qquad (7a)$$

where N_U is the ultimate number of cycles for which fatigue strength is very small, N_O is a reference number of cycles for which fatigue strength is very large, N is the current number of cycles the material has undergone, and s is the empirical material constant for the high-cycle mechanical fatigue effect. An initial estimate of 1×10^{10} was used for the ultimate number of cycles, N_U, since mechanical fatigue data beyond this value was not found for Inconel 718. An initial estimate of 0.5 or half a cycle was used for the reference number of cycles, N_O. Substitution of these values into equation (7a) results in the high-cycle mechanical fatigue model for Inconel 718, as given below by equation (7b).

$$\frac{S}{S_O} = \left[\frac{10^{10} - 0.5}{10^{10} - N}\right]^{-s} \qquad (7b)$$

Since the high-cycle fatigue domain is associated with lower loads and longer lives, or high numbers of cycles to failure (greater than 10^4 or 10^5 cycles), data consisting of cycle values less than 5×10^4 fall into the low-cycle fatigue regime and therefore, may be modeled by the low-cycle mechanical fatigue model presented in Section 4.3.

4.3 Low-Cycle Mechanical Fatigue Model

Equation (5), when modified for the effect of low-cycle mechanical fatigue, becomes:

$$\frac{S}{S_o} = \left[\frac{N''_U - N''_O}{N''_U - N''}\right]^{-r} , \qquad (8a)$$

where N''_U is the ultimate number of cycles for which fatigue strength is very low, N''_O is a reference number of cycles for which fatigue strength is very high, N'' is the current number of cycles the material has undergone, and r is the empirical material constant for the low-cycle mechanical fatigue effect. An initial estimate of 1×10^5 was used for the ultimate number of cycles, N''_U, since mechanical fatigue cycle values beyond this value fall into the high-cycle fatigue domain. An initial estimate of 0.5 or half a cycle was used for the reference number of cycles, N''_O. Substitution of these values into equation (8a) results in the low-cycle mechanical fatigue model for Inconel 718, as given below by equation (8b).

$$\frac{S}{S_o}=\left[\frac{1\times10^5-0.5}{1\times10^5-N^{'}}\right]^{-r} \tag{8b}$$

4.4 Creep Model

Equation (5), when modified for the effect of creep, becomes:

$$\frac{S}{S_O}=\left[\frac{t_U-t_O}{t_U-t}\right]^{-v}, \tag{9a}$$

where t_U is the ultimate number of creep hours for which rupture strength is very small, t_O is a reference number of creep hours for which rupture strength is very large, t is the current number of creep hours, and v is the empirical material constant for the effect of creep. An initial estimate of 1×10^6 was used for the ultimate number of creep hours, t_U, due to the fact that creep rupture life data beyond this value was not found for Inconel 718. An initial estimate of 0.25 hours or fifteen minutes was used for the reference number of creep hours, t_O. Substitution of these values into equation (9a) results in equation (9b) below.

$$\frac{S}{S_O}=\left[\frac{10^6-0.25}{10^6-t}\right]^{-v} \tag{9b}$$

4.5 Thermal Fatigue Model

The fifth and final effect for which Inconel 718 data was obtained is thermal fatigue. Thermal fatigue has been extensively discussed in the literature [10, 17, 24]. When modified for the effect of thermal fatigue, equation (5) becomes:

$$\frac{S}{S_O}=\left[\frac{N_U^{'}-N_O^{'}}{N_U^{'}-N^{'}}\right]^{-u}, \tag{10a}$$

where N'_U is the ultimate number of thermal cycles for which thermal fatigue strength is very small, N'_O is a reference number of thermal cycles for which thermal fatigue strength is very large, N' is the current number of thermal cycles the material has undergone, and u is an empirical material constant that represents the slope of a straight line fit of the modeled data on log-log paper.

Thermal fatigue is in the regime of low-cycle fatigue (less than 10^4 or 10^5 cycles), therefore, an intermediate value of 5×10^4 cycles was an initial estimate for the ultimate number of thermal fatigue cycles, N'_U. An initial estimate of 0.5 or half a cycle was used for the reference number of cycles, N'_O. Substitution of these values into equation (10a) results in the thermal fatigue model for Inconel 718, as given by equation (10b) below.

$$\frac{S}{S_O} = \left[\frac{5\times10^4 - 0.5}{5\times10^4 - N'}\right]^{-u} \qquad (10b)$$

4.6 Model Transformation

In the case of high-cycle mechanical fatigue, low-cycle mechanical fatigue, creep and thermal fatigue, the current value and the reference value are small compared to the ultimate value. Therefore, regardless of the current value used, the term $\left[\frac{A_U - A}{A_U - A_O}\right]$ remains approximately constant. In order to sensitize the model for these four effects, the $\log_{10}$ of each value was used. As seen in Tables 3 through 6, this transformation significantly increases the sensitivity of a product term to the data used within it. In addition, this transformation results in better statistical linear regression fits of the data, as seen later in Figures 6, 9, 12 and 20 of Section 5. Hence, the general term $\left[\frac{A_U - A}{A_U - A_O}\right]$ was modified to the sensitized form, $\left[\frac{\log(A_U) - \log(A)}{\log(A_U) - \log(A_O)}\right]$, for these four effects. The program, PROMISS94, modifies the program, PROMISS, to allow for the sensitized form of these four effects.

Table 3 Non-sensitized and Sensitized Terms for High-Cycle Mechanical Fatigue Data.

Test Temperature, °F	Cycles, N	$\left[\frac{(10^{10})-(N)}{(10^{10})-(0.5)}\right]$	$\left[\frac{\log(10^{10})-\log(N)}{\log(10^{10})-\log(0.5)}\right]$
75	10^5	0.99999	0.485388
	10^6	0.9999	0.388311
	10^7	0.999	0.291233
	10^8	0.99	0.194155
1000	10^5	0.99999	0.485388
	10^6	0.9999	0.388311
	10^7	0.999	0.291233
	10^8	0.99	0.194155
1200	10^5	0.99999	0.485388
	10^6	0.9999	0.388311
	10^7	0.999	0.291233
	10^8	0.99	0.194155

Table 4 Non-sensitized and Sensitized Terms for Low-Cycle Mechanical Fatigue Data.

Test Temperature, °F	Cycles, N"	$\left[\frac{(10^5)-(N^*)}{(10^5)-(0.5)}\right]$	$\left[\frac{\log(10^5)-\log(N^*)}{\log(10^5)-\log(0.5)}\right]$
1000	200	0.998005	0.509141
	400	0.996005	0.452354
	600	0.994005	0.419135
	800	0.992005	0.395567
	1000	0.990005	0.377285
	2000	0.980005	0.320498
	4000	0.960005	0.263711
	6000	0.940005	0.230493
	8000	0.920005	0.206924
	10000	0.900005	0.188643
	20000	0.800004	0.131856

Table 5 Non-sensitized and Sensitized Terms for Creep Rupture Data.

Test Temperature, °F	Rupture Life, t, Hrs	$\left[\frac{(10^6)-(t)}{(10^6)-(0.25)}\right]$	$\left[\frac{\log(10^6)-\log(t)}{\log(10^6)-\log(0.25)}\right]$
1000	27.8	0.99997	0.69008
	133.2	0.99987	0.58701
	256.0	0.99974	0.54404
	814.9	0.99919	0.46787
	1731.0	0.99827	0.41831
	8473.0	0.99153	0.31384
	21523.6	0.97848	0.25251
1100	28.2	0.99997	0.68914
	62.0	0.99994	0.63732
	151.9	0.99985	0.57837
	367.5	0.99963	0.52025
	2327.6	0.99767	0.39883
	10606.2	0.98939	0.29906
	33990.7	0.96601	0.22245
1200	10.6	0.99999	0.75351
	30.8	0.99997	0.68334
	150.0	0.99985	0.57920
	747.2	0.99925	0.47357
	3131.5	0.99687	0.37931
	7263.0	0.99274	0.32397
	10232.0	0.98977	0.30143
1300	18.0	0.99998	0.71867
	70.5	0.99993	0.62887
	182.7	0.99982	0.56623
	476.8	0.99952	0.50313
	808.0	0.99919	0.46843
	2870.7	0.99713	0.38503
	6048.0	0.99395	0.33601

Table 6 Non-sensitized and Sensitized Terms for Thermal Fatigue Data.

Cycles, N'	$\left[\frac{(5\times10^4)-(N')}{(5\times10^4)-(0.5)}\right]$	$\left[\frac{\log(5\times10^4)-\log(N')}{\log(5\times10^4)-\log(0.5)}\right]$
45	0.999110	0.609151
140	0.997210	0.510568
750	0.985010	0.364782
9750	0.805008	0.141993

5.0 EXPERIMENTAL MATERIAL DATA

In order to calibrate or anchor the empirical material constants, a_i, in the multifactor equation to particular aerospace materials of interest, it is necessary to collect experimental data. Since actual experiments were not conducted as part of this research project, data for several effects were collected from the open literature.

5.1 Literature Search

Initially, a computerized literature search of nickel-base superalloys was conducted to obtain existing experimental data on various material properties. Useful data on high temperature, high-cycle mechanical fatigue and creep properties were found for several nickel-base superalloys [2, 11, 15, 23]. Based on this data, a second computerized literature search of the superalloy, Inconel 718, was later performed in an attempt to find additional data, especially data on thermal fatigue effects. Efforts were concentrated on this particular superalloy for two primary reasons. First, Inconel 718 was selected as the initial material to be analyzed due to its extensive utilization by the aircraft and aerospace industries owing to its high performance properties. Secondly, data on Inconel 718 was far more abundant than for any other superalloy. As a result, data for four effects, namely, high temperature, high-cycle mechanical fatigue, low-cycle mechanical fatigue and creep were readily obtained. Data on thermal fatigue properties, however, was much harder to obtain. Therefore, a third computerized literature search for Inconel 718 thermal fatigue data was required. This search yielded limited thermal fatigue data for Inconel 718.

5.2 Inconel 718

Inconel 718 is a precipitation-hardenable nickel-chromium alloy containing significant amounts of iron, niobium and molybdenum along with lesser amounts of aluminum and titanium. It combines corrosion resistance and high strength with outstanding weldability. Inconel 718 has excellent creep-rupture strength and a high fatigue endurance limit up to 1300 °F (700 °C). It requires a somewhat complex heat treatment (solution anneal, cool and duplex age) to produce its high strength properties. Standard production forms are round, flats, extruded section, pipe, tube, forging stock, plate, sheet, strip and wire. Inconel 718 material in various forms is used in gas turbines, rocket engines (including the space shuttle main engine), spacecraft structural components, nuclear reactors, pumps and tooling. In gas turbine engines, for example, components operate under rigorous conditions of stress and temperature. The high performance superalloy, Inconel 718, is capable of meeting such extreme material requirements.

5.3 Temperature Data

The data on high temperature tensile strength properties of Inconel 718 resulted from tests conducted on hot-rolled round specimens annealed at 1950 °F and aged. [15]. This data, as well as the data on high-cycle mechanical fatigue, creep, and thermal fatigue strength properties, were plotted in various forms, one of which was the same as that used by the multifactor equation in PROMISS. The data plotted in Figures 2 and 3 show the effect of temperature on yield strength for Inconel 718. Figure 2 displays the raw data, while Figure 3 shows the data in the form given by equation (6b). As expected, the yield strength of the material decreases as the temperature increases. Linear regression of the data, as seen in Figure 3, produced a first estimate of the empirical material constant, q, for the temperature effect. This estimated value of the material constant, q, is given by the slope of the linear regression fit. As seen by Figure 3 and corroborated by the high R^2 (coefficient of determination [3]) value, this temperature data, when modeled by equation (6b), does indeed indicate a good linear relation between yield strength and temperature.

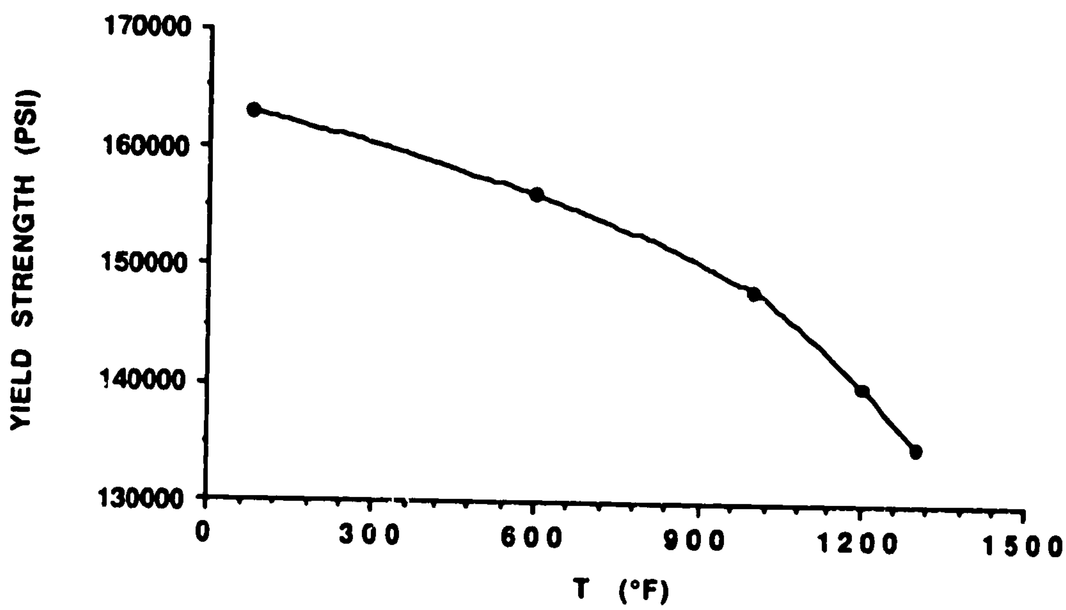

Fig. 2 Effect of Temperature (°F) on Yield Strength for Inconel 718.

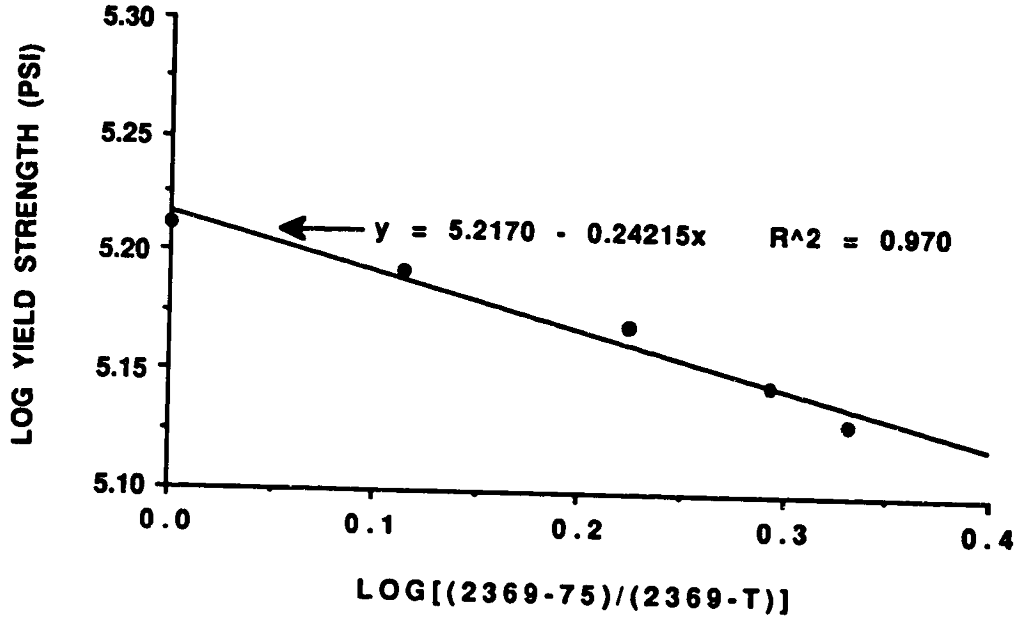

Fig. 3 Effect of Temperature (°F) on Yield Strength for Inconel 718.
(Log-Log Plot with Linear Regression)

5.4 High-Cycle Mechanical Fatigue Data

The data on high-cycle mechanical fatigue strength properties resulted from fatigue tests conducted on hot-rolled bar specimens annealed at 1750 °F and aged [15]. This data was plotted in various forms, including non-sensitized and sensitized model forms. Figure 4 presents the raw high-cycle mechanical fatigue data and displays the effect of mechanical fatigue cycles on fatigue strength for given test temperatures. As expected, the fatigue strength of Inconel 718 decreases as the number of cycles increases. Figures 5 and 6 show the data in the non-sensitized form of equation (7b) and the sensitized model form, respectively. Linear regression of the data produced first estimates of the empirical material constant, s, for the high-cycle mechanical fatigue effect, as given by the slopes of the linear regression fits. As seen by these regression fits in Figures 5 and 6, the R^2 (goodness of fit) values are significantly higher for the sensitized model form.

In reference to Figure 6, the R^2 value corresponding to a temperature of 75 °F is significantly lower than the fits calculated at temperatures of 1000 °F and 1200 °F. In addition, whereas the slope corresponding to a temperature of 1000 °F is lower than that corresponding to 1200 °F, the slope obtained at a temperature of 75 °F (s = 0.37848) is higher than that at both 1000 °F (s = 0.22348) and 1200 °F (s = 0.35425). This is due to the fact that at certain current cycle values, N, the fatigue strength at a temperature of 75 °F is lower than that at 1000 °F. Since this phenomenon is highly improbable, the validity of the high-cycle mechanical fatigue data obtained at a test temperature of 75 °F is questionable. Thus, the corresponding high-cycle mechanical fatigue material constant (s = 0.37848) is also questionable.

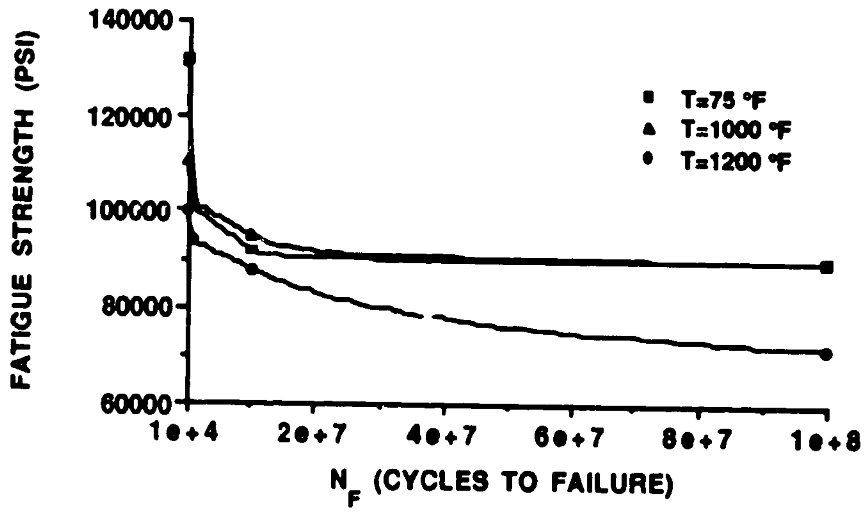

Fig. 4 Effect of High-Cycle Mechanical Fatigue (Cycles) on Fatigue Strength for Inconel 718.

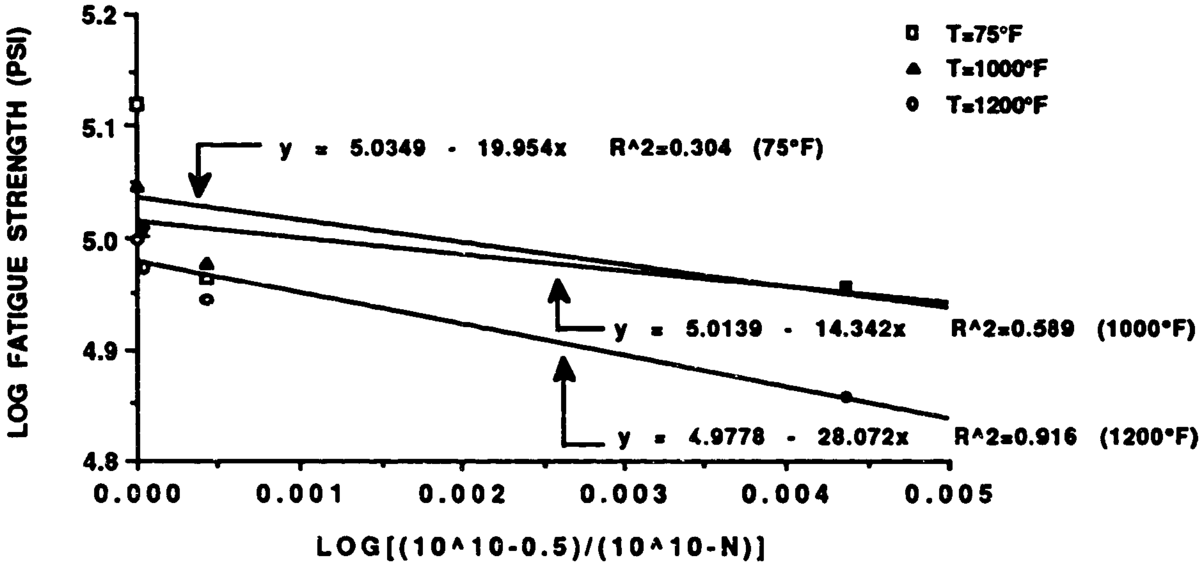

Fig. 5 Effect of High-Cycle Mechanical Fatigue (Cycles) on Fatigue Strength for Inconel 718.
(Non-sensitized Model Form)

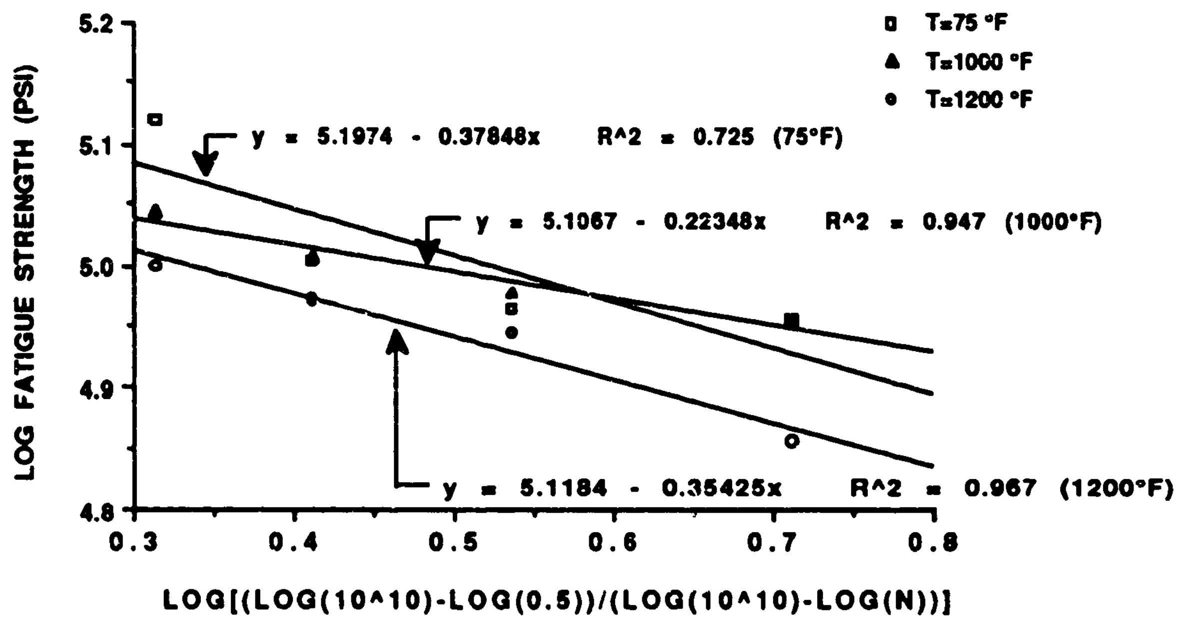

Fig. 6 Effect of High-Cycle Mechanical Fatigue (Cycles) on Fatigue Strength for Inconel 718.
(Sensitized Model Form)

5.5 Low-Cycle Mechanical Fatigue Data

The general model for the low-cycle mechanical fatigue effect uses stress-life (σ-N) data obtained from experimental strain-life (ε-N) data. The low-cycle mechanical fatigue data presented in Table 4 resulted from closed-loop strain controlled tests performed in air with induction heating [7]. These tests were conducted at a constant temperature of 1000 °F and a strain rate of 4×10^{-3} sec^{-1}.

By equation (11), the stress amplitude, $\Delta\sigma/2$, was calculated using the elastic strain and an average value of $E=24.5\times10^6$ psi (modulus of elasticity for Inconel 718 at 1000 °F) [15].

$$\frac{\Delta\sigma}{2}=E\left[\frac{\Delta\varepsilon_e}{2}\right] \qquad (11)$$

The resulting low-cycle mechanical fatigue stress-life (σ-N) data were plotted in various forms, including non-sensitized and sensitized model forms. Figure 7 presents the low-cycle mechanical fatigue data and shows the effect of mechanical fatigue cycles on stress amplitude at failure (i.e., fatigue strength) for the given test temperature of 1000 °F. As with the high-cycle mechanical fatigue data, the fatigue strength of Inconel 718 decreases as the number of cycles increases. Figures 8 and 9 show the data in the non-sensitized form of equation (8b) and the sensitized model form, respectively. Linear regression of the data produced a first estimate of the empirical material constant, r, for the low-cycle mechanical fatigue effect, as given by the slope of the linear regression fit. As seen by the regression fit in Figures 8 and 9, the R^2 (goodness of fit) value is significantly higher for the sensitized model form.

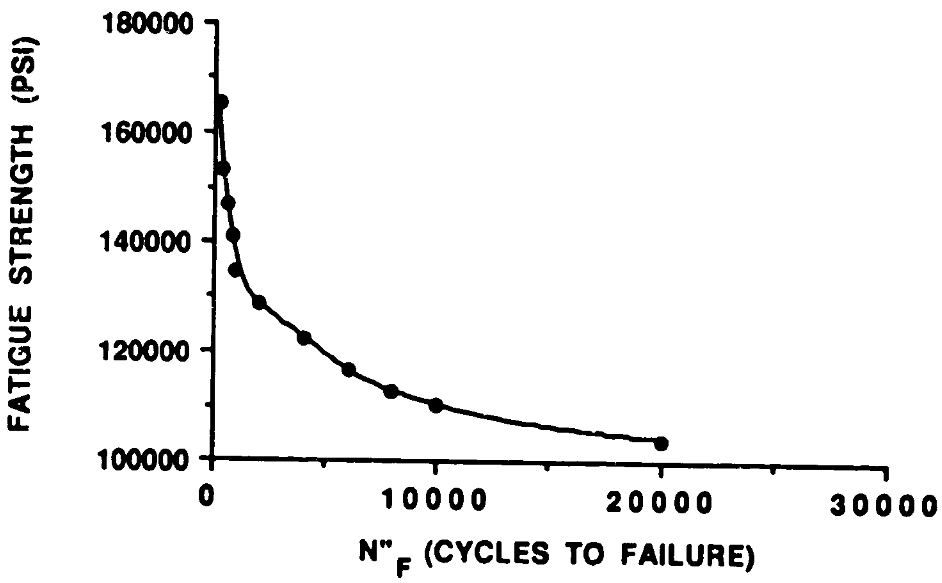

Fig. 7 Effect of Low-Cycle Mechanical Fatigue (Cycles) on Fatigue Strength for Inconel 718.

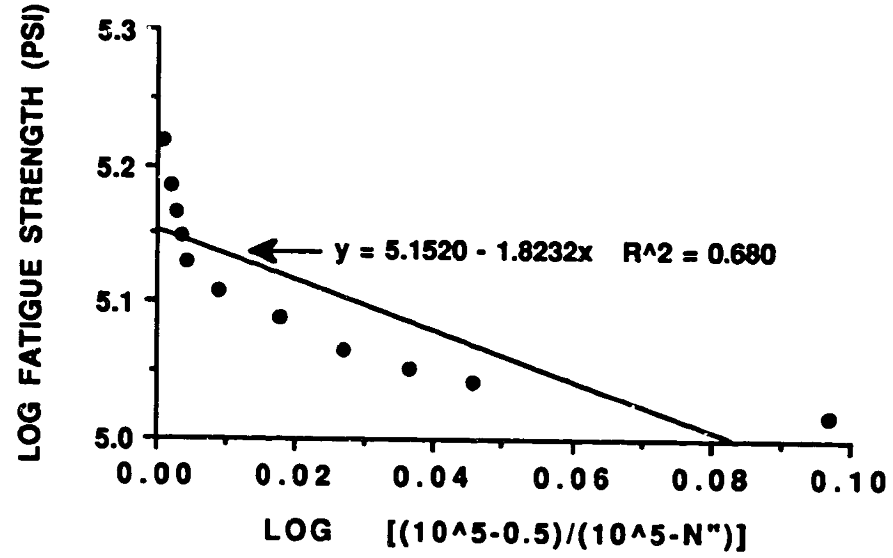

Fig. 8 Effect of Low-Cycle Mechanical Fatigue (Cycles) on Fatigue Strength for Inconel 718. (Non-sensitized Model Form)

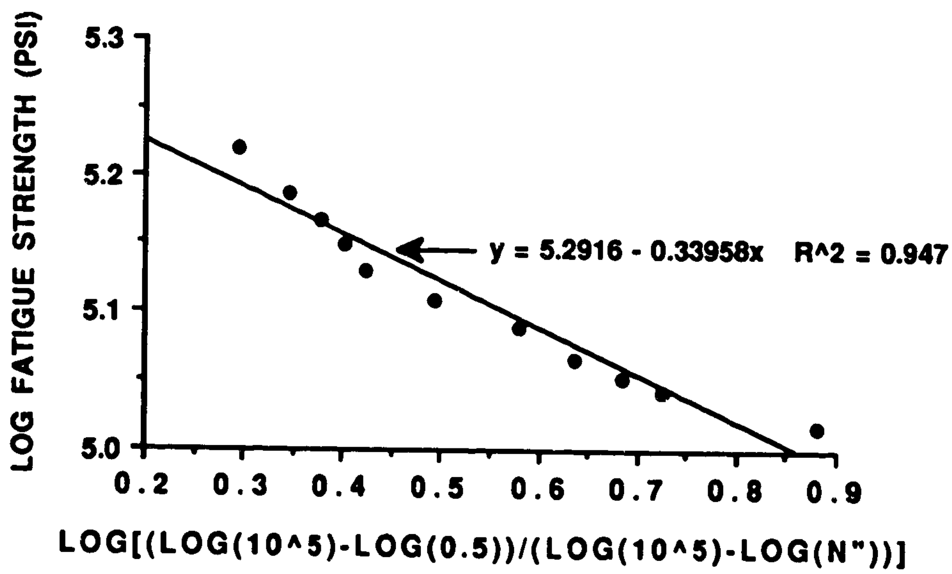

Fig. 9 Effect of Low-Cycle M^chanical Fatigue (Cycles) on Fatigue Strength for Inconel 718. (Sensitized Model Form)

5.6 Creep Rupture Data

The data on creep rupture strength properties resulted from tests conducted on stress rupture test bars annealed at 1800 °F and aged [2]. As with the mechanical fatigue data, this data was plotted in various forms. Figure 10 presents the raw creep rupture strength data and shows the effect of creep time on rupture strength for given test temperatures. Once again, the strength of the material decreases as the variable, in this case time, increases. In addition, for a given time, t, the rupture strength decreases as the test temperature increases. This phenomenon is clearly seen in Figure 10, as well as, by the changing slopes of the linear regression fits in Figures 11 and 12. Figures 11 and 12 show the creep data in the non-sensitized form of equation (9b) and the sensitized model form, respectively. Linear regression of the data produced first estimates of the empirical material constant, v, for the creep effect, as given by the slopes of the linear regression fits. As seen by these regression fits in Figures 11 and 12, the R^2 (goodness of fit) value is significantly higher for the sensitized model form.

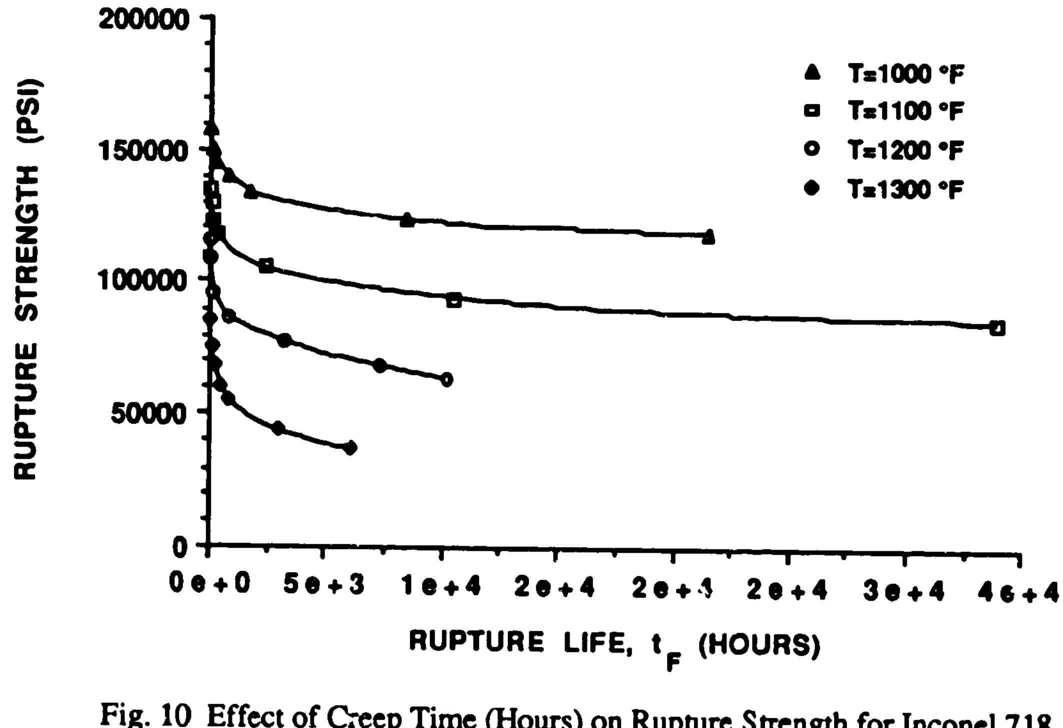

Fig. 10 Effect of Creep Time (Hours) on Rupture Strength for Inconel 718.
(Linear Plot)

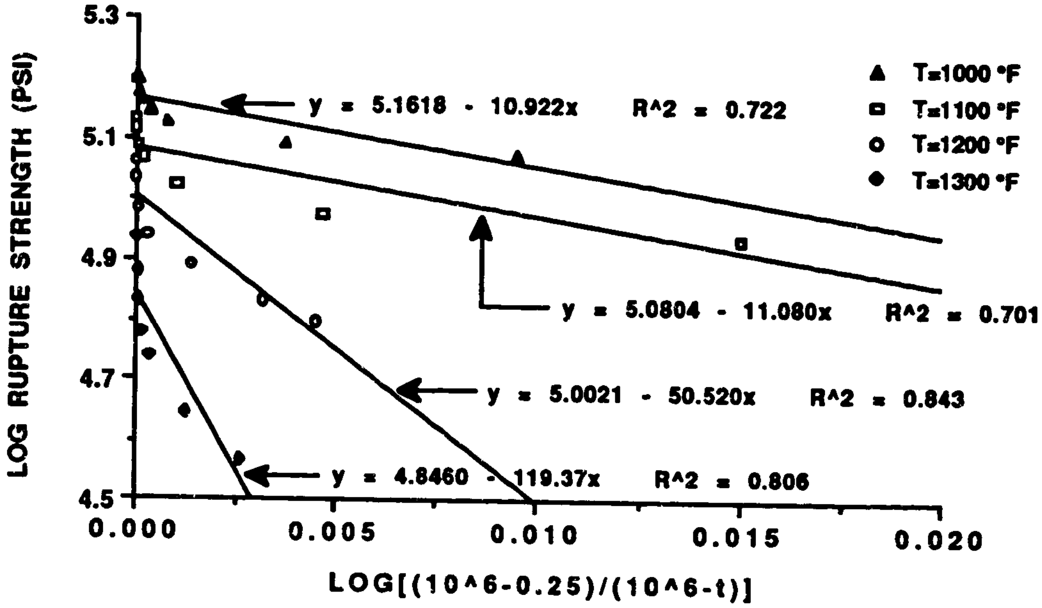

Fig. 11 Effect of Creep Time (Hours) on Rupture Strength for Inconel 718.
(Non-sensitized Model Form)

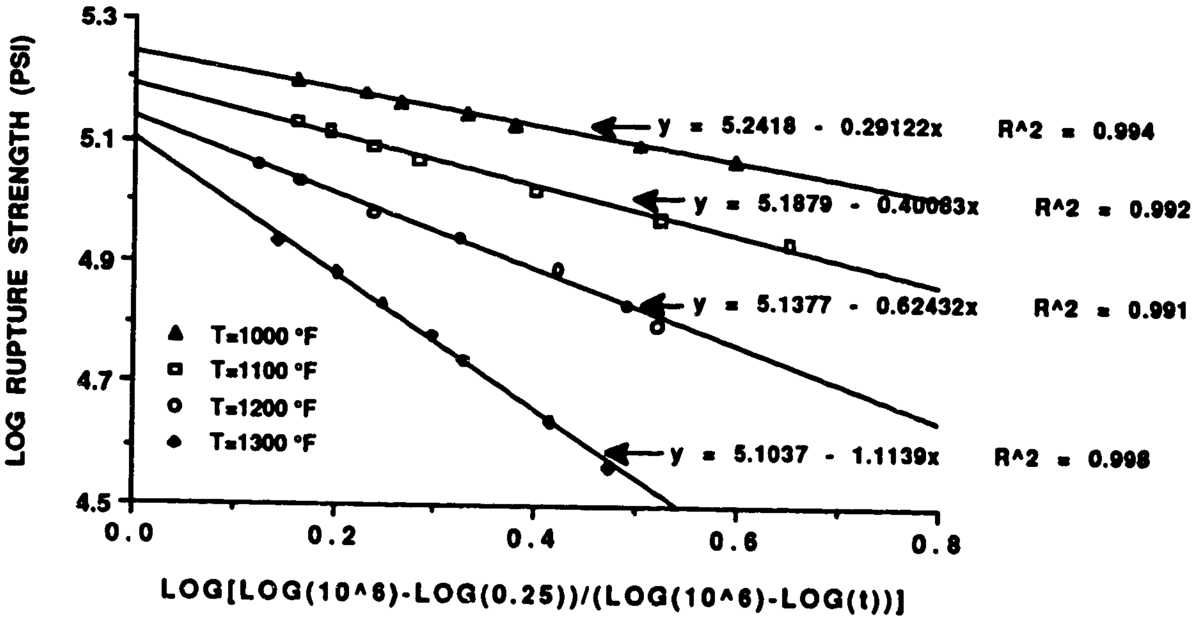

Fig. 12 Effect of Creep Time (Hours) on Rupture Strength for Inconel 718.
(Sensitized Model Form)

5.7 Thermal Fatigue Data

Low cycle fatigue produces cumulative material damage and ultimate failure in a component by the cyclic application of strains that extend into the plastic range. Failure typically occurs under 10^4 or 10^5 cycles. Low cycle fatigue is often produced mechanically under isothermal conditions. However, machine components may also be subjected to low-cycle fatigue due to a cyclic thermal field. These cyclic temperature changes produce thermal expansions and contractions that, if constrained, produce cyclic stresses and strains. These thermally induced stresses and strains result in fatigue failure in the same manner as those produced mechanically.

The general model for the thermal fatigue effect uses stress-life (σ-N) data obtained from experimental strain-life (ε-N) data. The thermal fatigue data presented in Table 7 resulted from thermomechanical fatigue tests conducted on test bars annealed at 1800 °F and aged [17]. The temperature and strain were computer-controlled by the same triangular waveform with in-phase cycling at a frequency of 0.0056 Hz.. The temperature was cycled between a minimum temperature of 600 °F and a maximum temperature of 1200 °F, with a mean temperature of approximately 900 °F. This total strain amplitude data and plastic strain amplitude data were used to construct the strain-life curves presented in Figure 13.

Table 7 Thermal Fatigue Data for Inconel 718.

Cycles to Failure N'_F	Total Strain Amplitude, $\Delta\varepsilon_T/2$	Plastic Strain Amplitude, $\Delta\varepsilon_P/2$	Stress Amplitude, $\Delta\sigma/2$ (psi)
45	0.0100	0.0050	126,500
140	0.0075	0.0029	116,380
750	0.0050	0.0011	98,670
9750	0.0040	0.0003	93,610

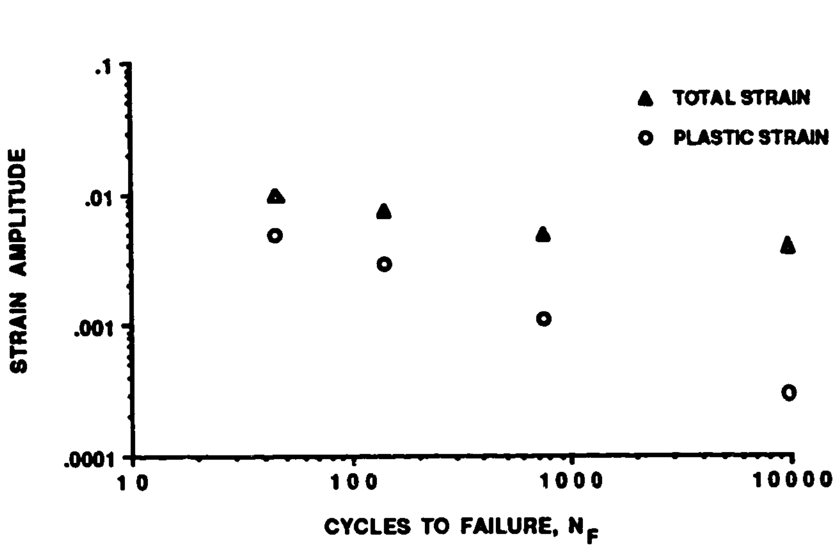

Fig. 13 Strain-life Curve for Inconel 718.

By equation (12), the stress amplitude, $\Delta\sigma/2$, was calculated using total and plastic strain amplitudes, $\Delta\varepsilon_T/2$ and $\Delta\varepsilon_P/2$, respectively, along with an average value of $E=25\times10^6$ psi (modulus of elasticity for Inconel 718 at 900 °F) [15].

$$\frac{\Delta\sigma}{2} = E\left[\frac{\Delta\varepsilon_T}{2} - \frac{\Delta\varepsilon_P}{2}\right] \qquad (12)$$

The resulting stress amplitude data were then plotted against the plastic strain amplitude data to produce the cyclic stress-strain curve shown below in Figure 14.

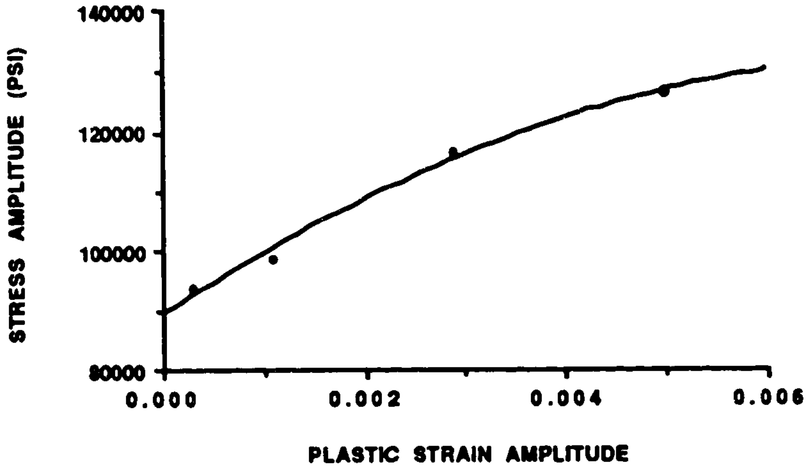

Fig. 14 Cyclic Stress-Strain Curve for Inconel 718.

Using power law regression techniques [1] and the data in Table 7, fatigue properties for Inconel 718 were calculated. These properties were calculated and compared with known established values in order to check the validity of the data. The plastic portion of the strain-life curve (Figure 13) may be represented by the following power law function:

$$\frac{\Delta\varepsilon_P}{2} = \varepsilon_F^{'}\left(2N_F^{'}\right)^c , \tag{13}$$

where $\Delta\varepsilon_P/2$ is the plastic strain amplitude and $2N'_F$ are the reversals to failure. A power law regression analysis of the data yielded two fatigue properties, namely, the fatigue ductility coefficient, ε'_F, and the fatigue ductility exponent, c. These two properties are indicated graphically, along with their coefficient of determination, R^2, in Figure 15. Regression statistics, such as R^2, were obtained to indicate whether or not a power law representation of the relationship between plastic strain amplitude and reversals to failure was appropriate. As confirmed by the high R^2 value in Figure 15, the power law function of equation (11) well represents the relationship between $\Delta\varepsilon_P/2$ and $2N'_F$.

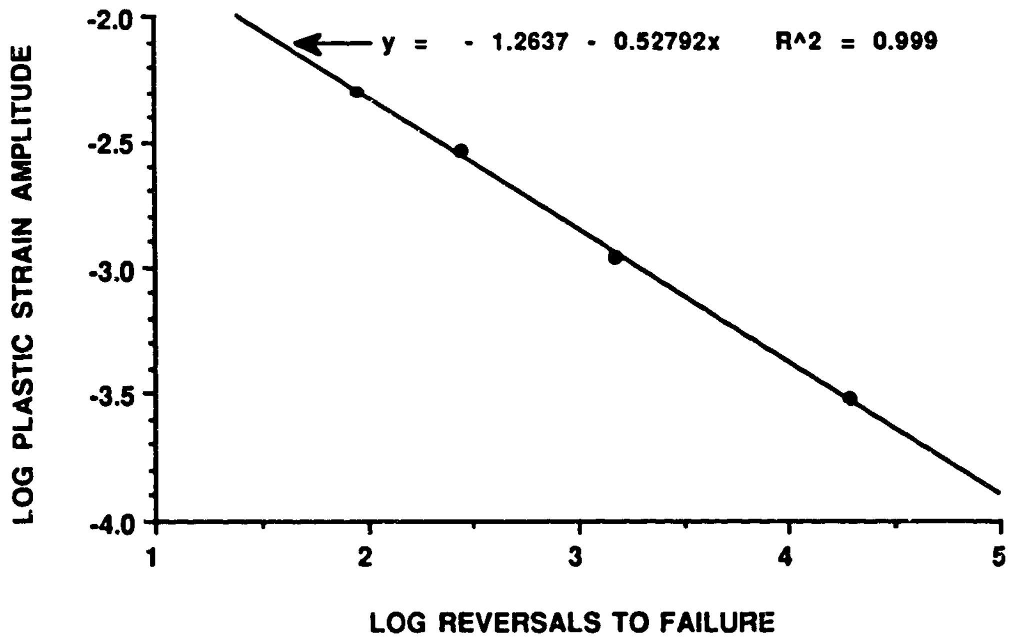

Fig. 15 Regression of Equation (11) Data Yielding Fatigue Ductility Coefficient, ε'_F, and Fatigue Ductility Exponent, c.

The following power law function was satisfactory for expressing the cyclic stress-strain relationship of the data presented in Figure 14:

$$\frac{\Delta\sigma}{2} = K'\left(\frac{\Delta\varepsilon_P}{2}\right)^{n'} \quad . \tag{14}$$

Regression analysis of this data yielded two more fatigue properties, K', the cyclic strength coefficient and n', the cyclic strain hardening exponent. These two properties are indicated graphically, along with their coefficient of determination, R^2, in Figure 16.

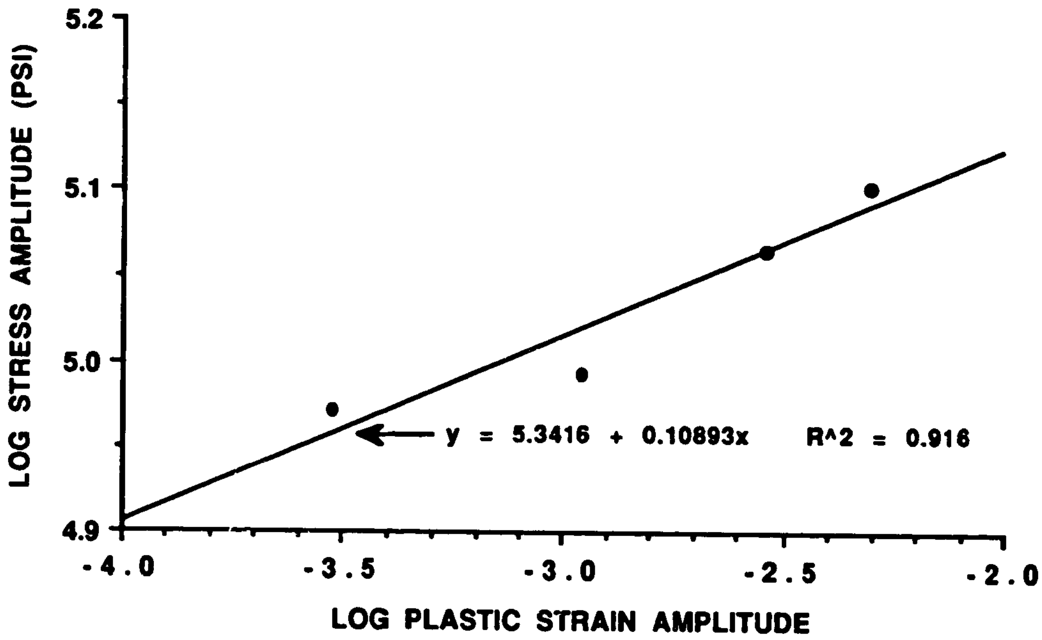

Fig. 16 Regression of Equation (12) Data Yielding Cyclic Strength Coefficient, K', and Cyclic Strain Hardening Exponent, n'.

The following power law function was used to approximate the relationship between stress amplitude and reversals to failure:

$$\frac{\Delta\sigma}{2} = \sigma'_F\left(2N'_F\right)^b \quad . \tag{15}$$

Regression analysis of this data yielded two more fatigue properties, σ'_F, the fatigue strength coefficient and b, the fatigue strength exponent. These two properties are indicated graphically, along with their coefficient of determination, R^2, in Figure 17. They complete the set of fatigue material properties calculated. The complete set of properties are given in Table 8, along with accepted ranges for the exponents [1].

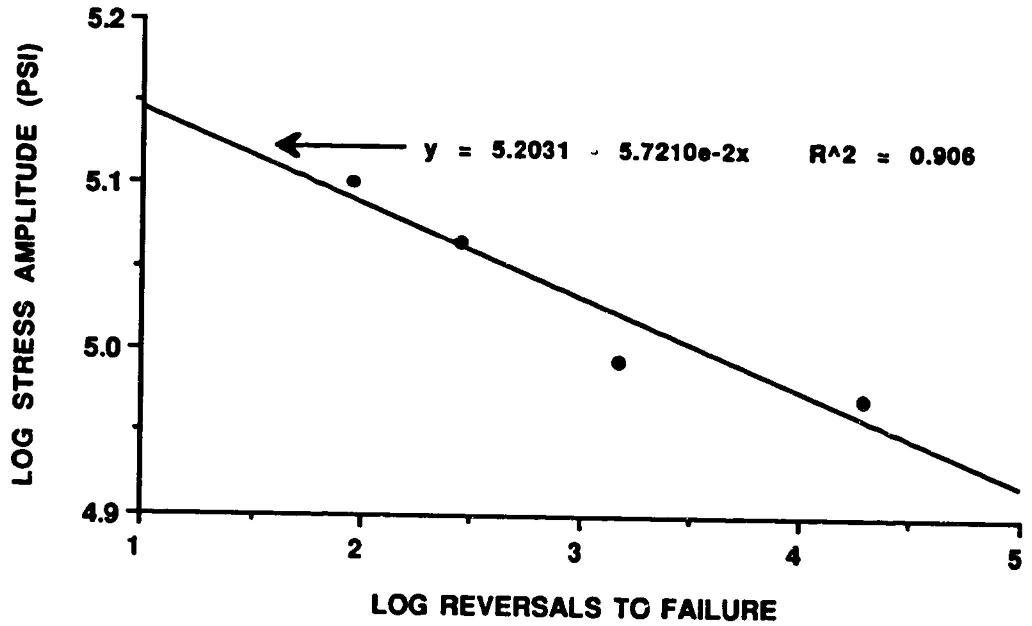

Fig. 17 Regression of Equation (13) Yielding Fatigue Strength Coefficient, σ'_F, and Fatigue Strength Exponent, b.

Table 8 Fatigue Material Properties for Inconel 718.

Material Property	Calculated Value	Accepted Range
Fatigue Ductility Coefficient, ε'_F	-1.2637 (0.0545)	
Fatigue Ductility Exponent, c	-0.5279	-0.5 to -0.7
Cyclic Strength Coefficient, K'	5.3416 (219,584 psi)	
Cyclic Strain Hardening Exponent, n'	0.1089	0.10 to 0.25
Fatigue Strength Coefficient, σ'_F	5.2031 (159,625 psi)	
Fatigue Strength Exponent, b	-0.0572	-0.05 to -0.12

The thermal fatigue stress-life (σ-N) data were plotted in various forms. Figure 18 presents the thermal fatigue data and displays the effect of thermal fatigue cycles on stress amplitude at failure (i.e., thermal fatigue strength) for a mean thermal cycling temperature of 900 °F. As expected, the thermal fatigue strength decreases as the number of cycles increases. Once again, the data was plotted in both non-sensitized and sensitized model forms to illustrate how the sensitized model results in a significant increase in the R^2 (goodness of fit) value. Figure 19 presents the data in the non-sensitized form of equation (10b), while Figure 20 shows the data in the sensitized model form. Linear regression of the data, as seen in Figure 20, produced a first estimate of the empirical material constant, u, for the thermal fatigue effect, as given by the slope of the linear regression fit.

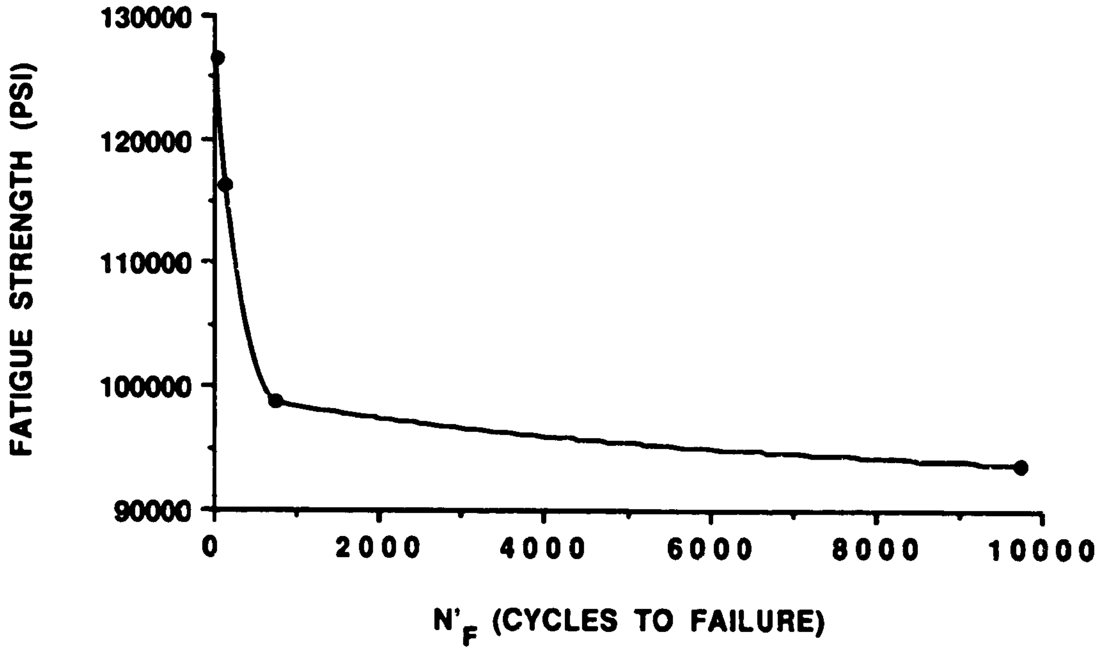

Fig. 18 Effect of Thermal Fatigue (Cycles) on Thermal Fatigue Strength (i.e., Stress Amplitude at Failure) for Inconel 718.

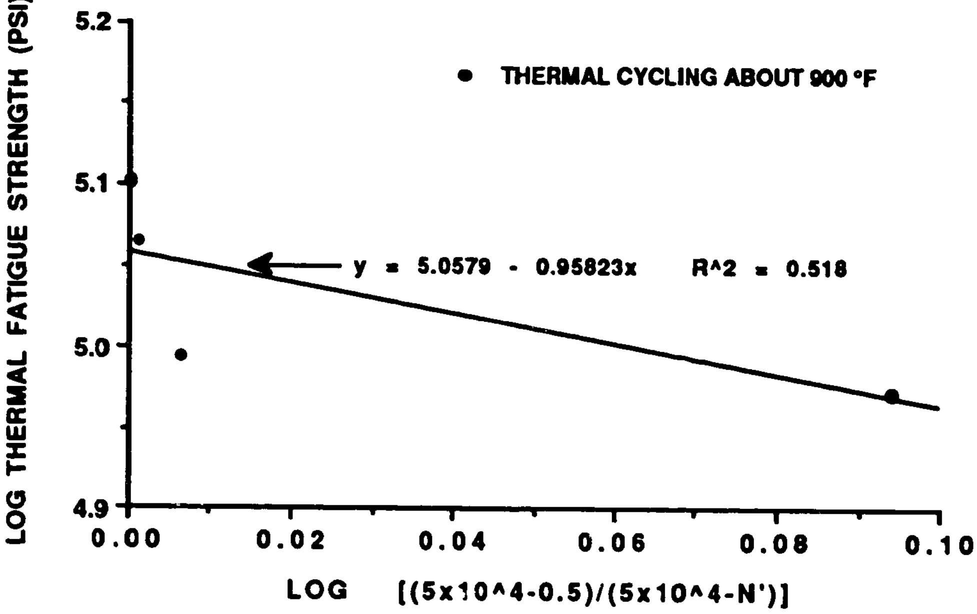

Fig. 19 Effect of Thermal Fatigue (Cycles) on Thermal Fatigue Strength. (Non-sensitized Model Form)

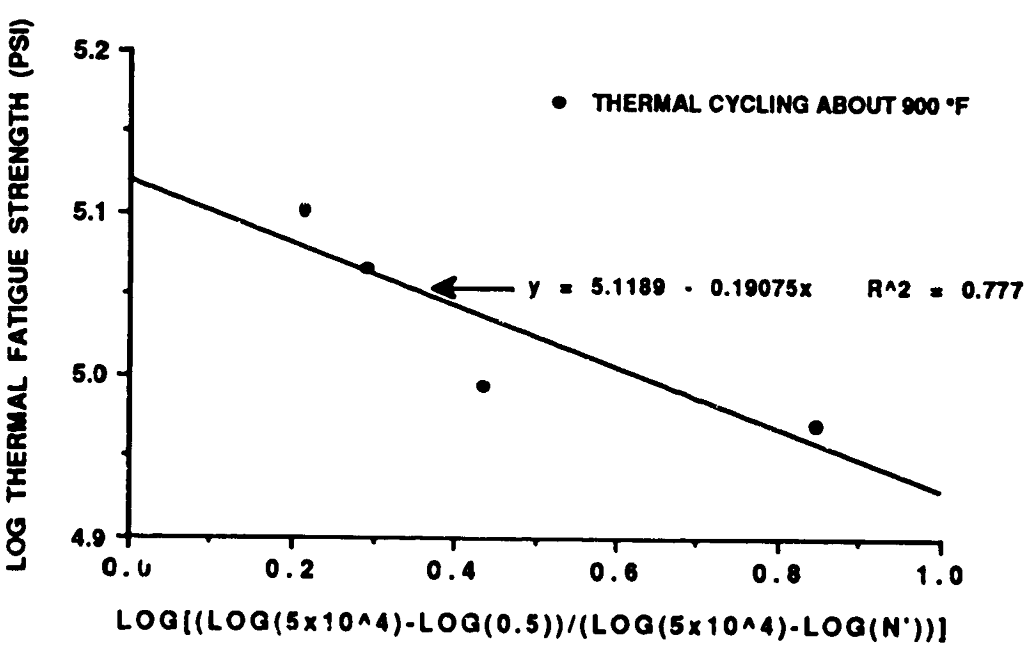

Fig. 20 Effect of Thermal Fatigue (Cycles) on Thermal Fatigue Strength. (Sensitized Model Form)

5.8 Model Calibration

The first estimates of the ultimate and reference values for each effect are given in Table 9. First estimates of the empirical material constants, previously determined from linear regression of high temperature, high-cycle mechanical fatigue, low-cycle mechanical fatigue, creep and thermal fatigue data, are summarized in Table 10. These initial estimates were used to calibrate the strength degradation model specifically for Inconel 718. Thus, model accuracy is dependent on proper selection of ultimate and reference values, which in turn influence the values of the empirical material constants.

Table 9 Initial Estimates for the Ultimate and Reference Values.

Effect	Ultimate Value Symbol	Estimated Ultimate Value	Reference Value Symbol	Estimated Reference Value
Temperature	T_U	2369	T_O	75
High-Cycle Mechanical Fatigue	N_U	1×10^{10}	N_O	0.5
Low-Cycle Mechanical Fatigue	N''_U	1×10-	N''_O	0.5
Creep	t_U	1×10^{6}	t_O	0.25
Thermal Fatigue	N'_U	5×10^{4}	N'_O	0.5

Table 10 Initial Estimates for the Empirical Material Constants.

Effect	Empirical Material Constant Symbol	Estimated Value of Constant	Applicable Temperature (°F)
High Temperature	q	0.2422	75-1300
High-Cycle Mechanical Fatigue	s	0.3785	75
High-Cycle Mechanical Fatigue	s	0.2235	1000
High-Cycle Mechanical Fatigue	s	0.3543	1200
Low-Cycle Mechanical Fatigue	r	0.3396	1000
Creep	v	0.2912	1000
Creep	v	0.4008	1100
Creep	v	0.6243	1200
Creep	v	1.1139	1300
Thermal Fatigue	u	0.2368	900

As previously mentioned, the quantities used for ultimate and reference values were initial estimates. Based on the parameters obtained from linear regression analysis of the data, i.e. slope (material constant), y-intercept (log S_O) and R^2, an attempt to adjust these initial estimates to improve the accuracy of the model was made. Noting that the y-intercept value corresponds to the log of the reference strength, S_O, it was necessary to physically define what the quantity S_O represents. For the temperature model, given the data used, S_O (5.217 or 164,816 psi) estimates the yield strength of Inconel 718 at the reference temperature of 75 °F as seen by Figure 3. In order to correlate the S_O for all effects to the yield strength, the ultimate and reference values for high-cycle and low-cycle mechanical fatigue, creep and thermal fatigue effects were adjusted. Adjusting the ultimate value influenced the slope, y-intercept and R^2 values, while adjusting the reference value altered the y-intercept value but had no affect on either the slope or R^2 values. In addition, certain trends were noted. Increasing the ultimate value increased the S_O value, while increasing the reference value decreased it.

Based on this information, initial estimates were reevaluated for high-cycle mechanical fatigue, low-cycle mechanical fatigue, creep and thermal fatigue effects.

Reevaluation of the initial estimates for the temperature effect was not necessary since this temperature data consisted of yield strength values at various temperatures, thus S_O is already correlated to a yield strength value of Inconel 718. For the high-cycle mechanical fatigue effect, Figure 6 shows log S_O values of 5.1974 (157,543 psi), 5.1067 (127,850 psi) and 5.1184 (131,341 psi) for temperatures of 75, 1000 and 1200 °F, respectively. According to average yield strength data for Inconel 718 [16], these values are too low. Therefore, in order to increase these y-intercept values, the ultimate value was varied between 1×10^{10} and 1×10^{11} cycles, while the reference value was varied between 0.5 and 0.25 cycles. The result was that an ultimate value of 1×10^{10} combined with a reference value of 0.25 yielded y-intercept values closest to the average yield strength for corresponding temperatures. Initial ultimate and reference values for the low-cycle mechanical fatigue, creep and thermal fatigue models were also adjusted accordingly. Figures 21, 22, 23 and 24, show the improved ultimate and reference values selected and display the subsequent new linear regression results of the high-cycle mechanical fatigue, low-cycle mechanical fatigue, creep and thermal fatigue data, respectively. Table 11 lists the improved estimates obtained for the ultimate and reference values, while Table 12 provides the corresponding new empirical material constants.

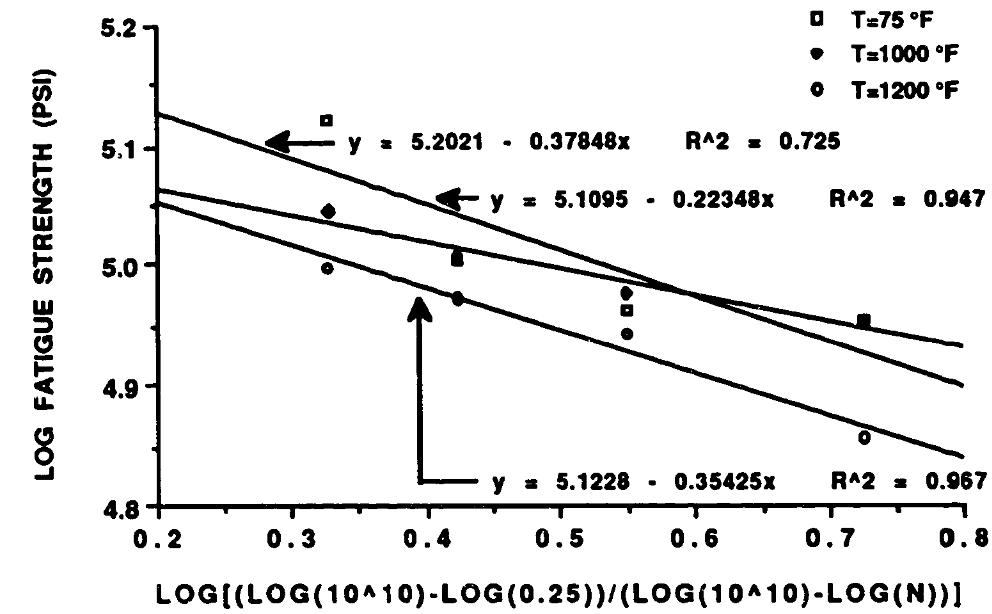

Figure 21 Effect of High-Cycle Mechanical Fatigue (Cycles) on Fatigue Strength for Inconel 718. (Sensitized Model Form Using Improved Estimates)

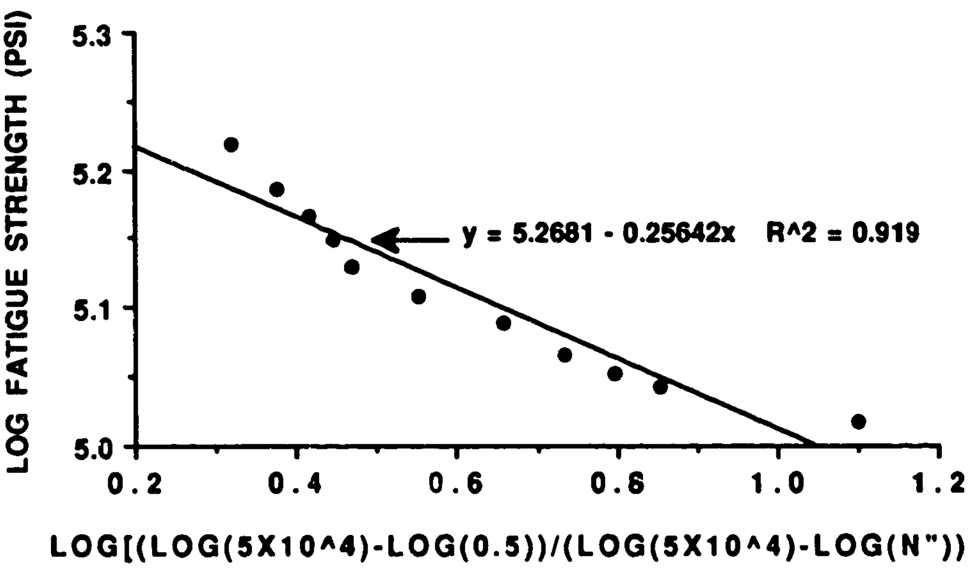

Figure 22 Effect of Low-Cycle Mechanical Fatigue (Cycles) on Fatigue Strength for Inconel 718. (Sensitized Model Form Using Improved Estimates)

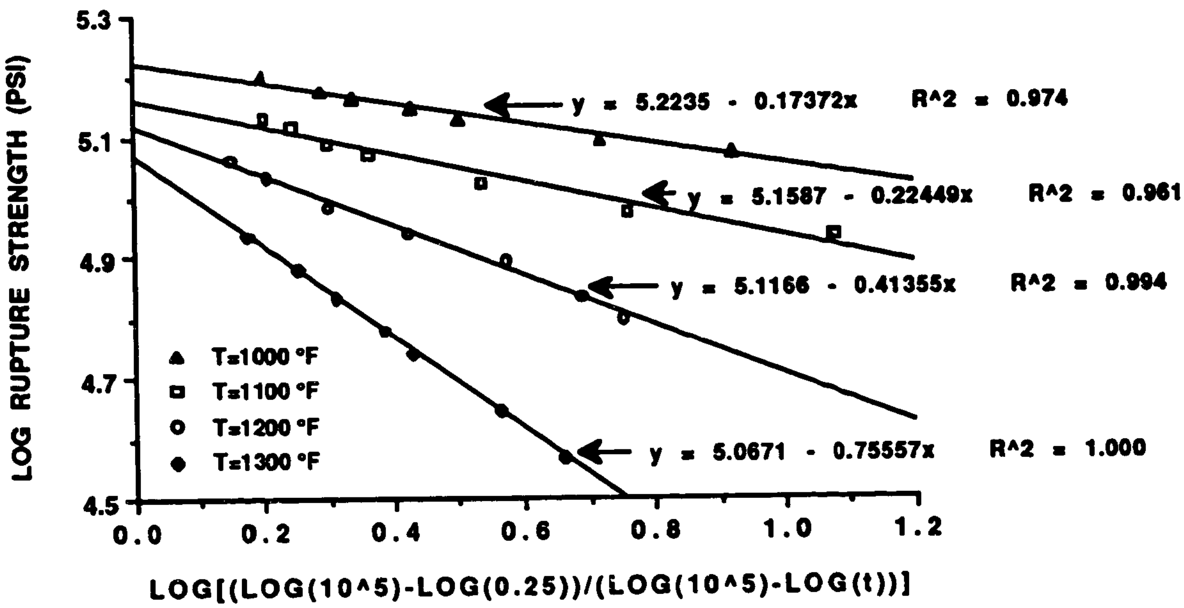

Figure 23 Effect of Creep Time (Hours) on Rupture Strength for Inconel 718.
(Sensitized Model Form Using Improved Estimates)

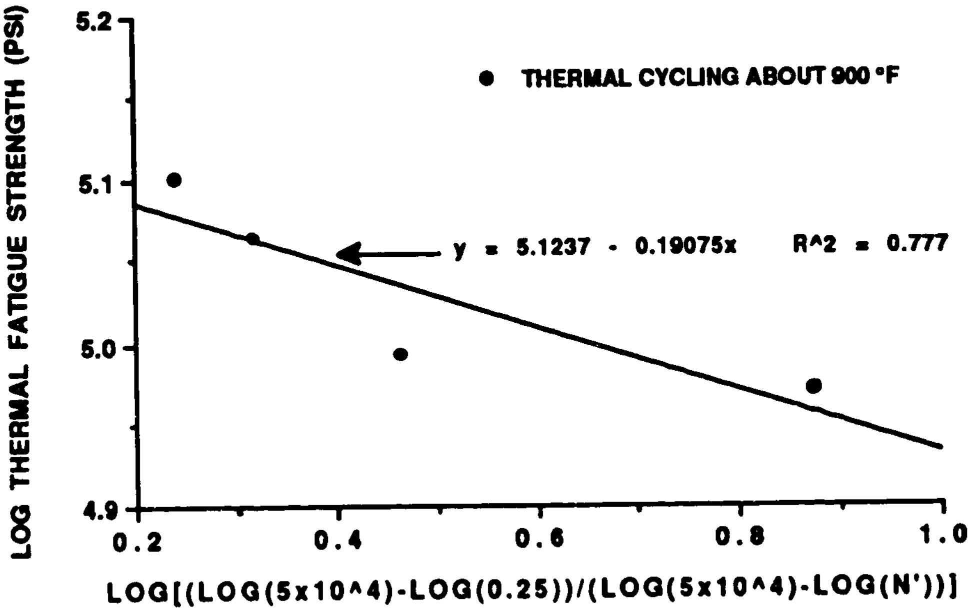

Figure 24 Effect of Thermal Fatigue (Cycles) on Thermal Fatigue Strength.
(Sensitized Model Form Using Improved Estimates)

Table 11 Improved Estimates for the Ultimate and Reference Values.

Effect	Ultimate Value Symbol	Estimated Ultimate Value	Reference Value Symbol	Estimated Reference Value
Temperature	T_U	2369	T_O	75
High-Cycle Mechanical Fatigue	N_U	1×10^{10}	N_O	0.25
Low-Cycle Mechanical Fatigue	N''_U	5×10^4	N''_O	0.50
Creep	t_U	1×10^5	t_O	0.25
Thermal Fatigue	N'_U	5×10^4	N'_O	0.25

Table 12 Improved Estimates for the Empirical Material Constants.

Effect	Empirical Material Constant Symbol	Estimated Value of Constant	Applicable Temperature (°F)
High Temperature	q	0.2422	75-1300
High-Cycle Mechanical Fatigue	s	0.3785	75
High-Cycle Mechanical Fatigue	s	0.2235	1000
High-Cycle Mechanical Fatigue	s	0.3543	1200
Low-Cycle Mechanical Fatigue	r	0.2564	1000
Creep	v	0.1737	1000
Creep	v	0.2245	1100
Creep	v	0.4136	1200
Creep	v	0.7556	1300
Thermal Fatigue	u	0.1908	900

6.0 ESTIMATION OF EMPIRICAL MATERIAL CONSTANT VARIABILITY

Due to a lack of sufficient data from which to evaluate the material constants, a_i, methodology to estimate the variability of these constants was developed. This methodology yields estimates for the standard deviations of the constants. For instance, when modeling high temperature effects, the material strength degradation model for Inconel 718 is given below by equation (6a).

$$\frac{S}{S_O} = \left[\frac{T_U - T_O}{T_U - T}\right]^{-q} \quad (6a)$$

or

$$S = S_O\left[\frac{T_U - T_O}{T_U - T}\right]^{-q} \quad (16a)$$

Taking the log of both sides yields equation (14b) below.

$$\text{Log } S = -q\left(\text{Log}\left[\frac{T_U - T_O}{T_U - T}\right]\right) + \text{Log } S_O \quad (16b)$$

It is clearly seen that equation (16b) is a linear equation with slope, -q, and y-intercept, Log S_O. Using the temperature data presented in Section 5, the linear relationship given by equation (16b) is shown graphically in Figure 25.

Linear regression of this temperature data yielded two parameters, the slope (-0.2422) and the y-intercept (5.2170). As previously discussed, the slope was used as a first estimate of the empirical material constant for the temperature degradation model. Due to limited temperature data, only five data points, concern over the accuracy of this estimated value was warranted. Therefore, steps were taken to model this material constant as a random variable so that an estimate of its standard deviation could be calculated.

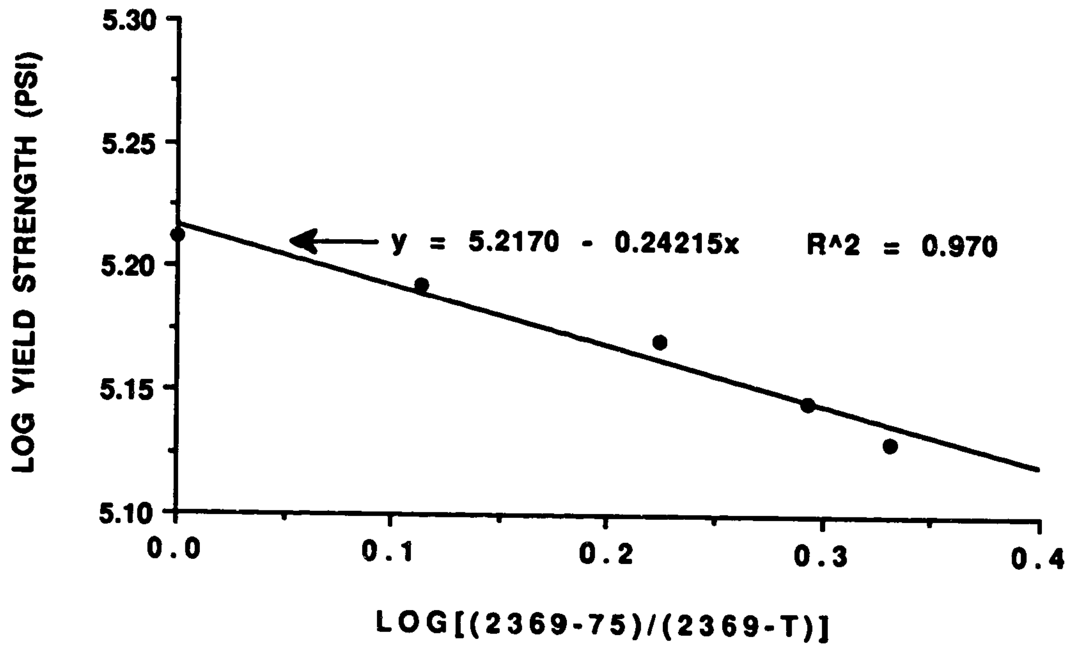

Figure 25 Linear Regression of Temperature Data.

First, maximum and minimum feasible slopes and y-intercepts were determined from consideration of the data and the linear regression results, such that these extreme parameters would theoretically enclose or envelope all actual data. Figure 26 shows the linear regression of the temperature data along with postulated maximum and minimum slopes. These extreme parameters were obtained by adjusting the slope of the linear regression fit. Rotating about the y-intercept value, the regression line was adjusted to pass through the outer most points, resulting in maximum and minimum slopes. Figure 27 shows the linear regression of the temperature data along with maximum and minimum y-intercepts. These extreme parameters were obtained by shifting the regression line vertically. While maintaining the slope, the regression line was shifted to pass through the outer most points, resulting in maximum and minimum y-intercept values.

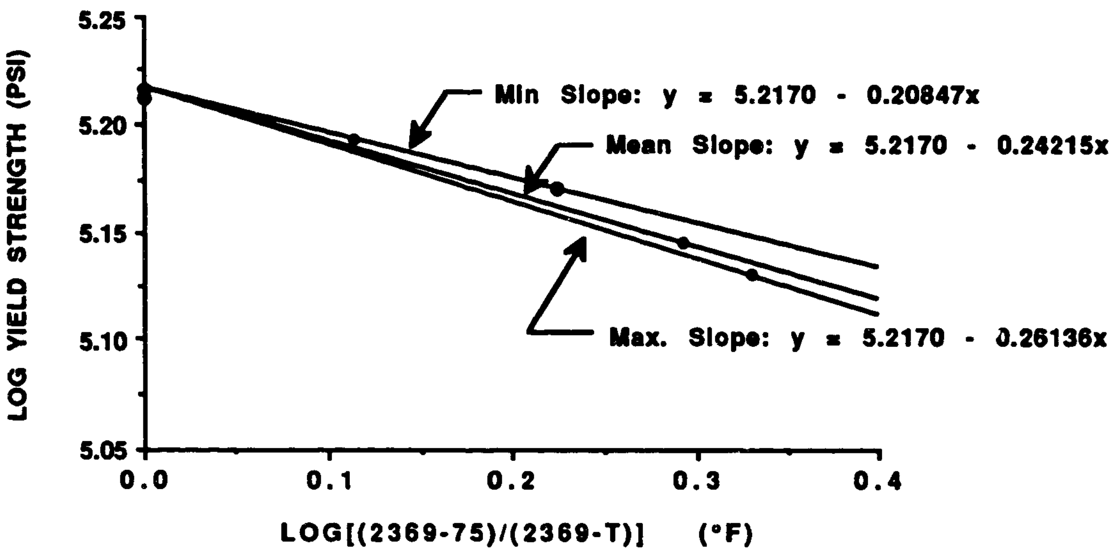

Figure 26 Postulated Maximum and Minimum Slopes.

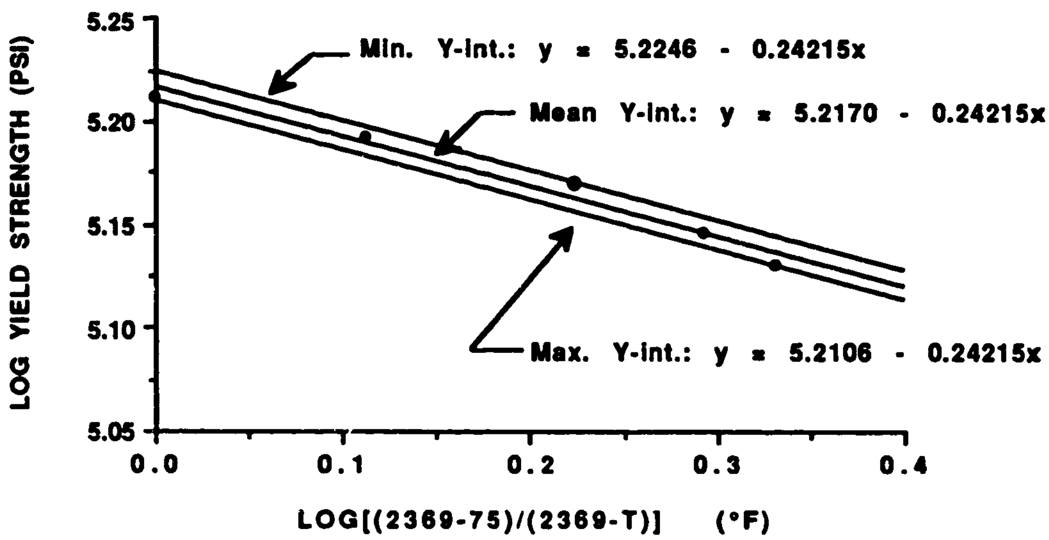

Figure 27 Postulated Maximum and Minimum Y-intercepts.

Using the values of the parameters obtained from linear regression along with the extreme maximum and minimum values, random variables for slope (-q) and y-intercept (log S_O) were constructed. These random parameters or variables were assumed to have normal distributions, with mean values given by the linear regression fit in Figure 25. Standard deviation values for the slope and y-intercept were determined using the extreme values together with the empirical rule. According to this rule, for a normal distribution, the mean value (μ) plus or minus three standard deviations ($\pm 3\sigma$) will contain 99.73% of the values [18, 21]. Therefore, the range of the values (maximum value minus the minimum value) divided by six yields the standard deviation, σ. Although the mean value resulting from linear regression (Figure 25) is not equal to μ (one-half the range) due to the nature of the data and the extreme values obtained, this method provides for an approximation of the standard deviation.

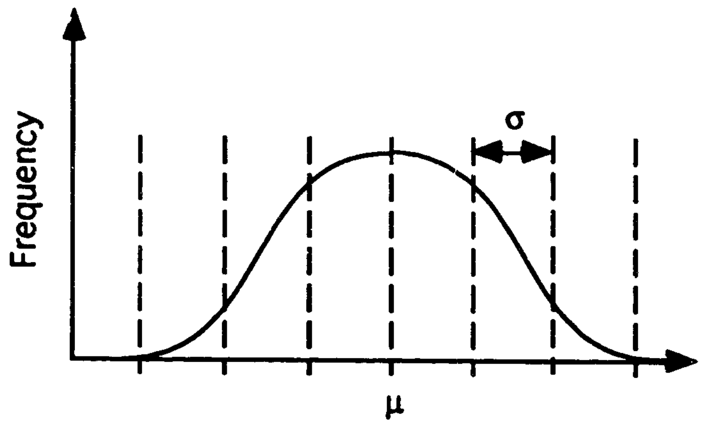

Figure 28 Probability Density Function of a Normal Distribution.

Values for the standard deviation of the random parameters, slope and y-intercept, were estimated as follows:

$$\sigma_{slope} = \frac{\text{maximum slope} - \text{minimum slope}}{6} = \frac{0.2614 - 0.2085}{6} = 0.0088$$

$$\sigma_{y\text{-int.}} = \frac{\text{maximum y-int.} - \text{minimum y-int.}}{6} = \frac{167{,}707.20 - 162{,}416.67}{6} = 881.75 \text{ (psi)}$$

These random parameters, now expressed in terms of their mean and standard deviation, were used to define the probabilistic material strength degradation model for temperature as a random parameter model having the following form:

$$S = S_O\left[\frac{T_U - T_O}{T_U - T}\right]^{-q} = S_O\left[\frac{2369-75}{2369-T}\right]^{-q} , \tag{16c}$$

where -q and S_O are now random variables for the slope and y-intercept, respectively.

In order to demonstrate this methodology, modifications were made to PROMISS [6]. These modifications included providing random variable input mechanisms for S_O in terms of its mean and standard deviation, adding random number generation capability for S_O, and providing coding to calculate equation (16c), so that results are given in terms of strength, S, rather than lifetime strength, S/S_O. The resulting values for S were calculated by simulation using an augmented version of PROMISS called CALLIE92T. Forty values of strength, S, corresponding to each temperature value, T, were obtained. Figure 29 displays selected strength values of the forty calculated, along with the actual temperature data and the postulated envelope of the random parameter model as defined by the extreme parameter values. The statistical frequency with which calculated values of S fell within the envelope were noted. Since an overwhelmingly large number of S values were found to lie within the envelope, it was ascertained that experimental temperature data beyond the known five data points would also fall within the envelope. Thus, this estimated value of the standard deviation, rather than expert opinion or an assumed value, can be used with greater confidence in the probabilistic material strength degradation model embodied in PROMISS.

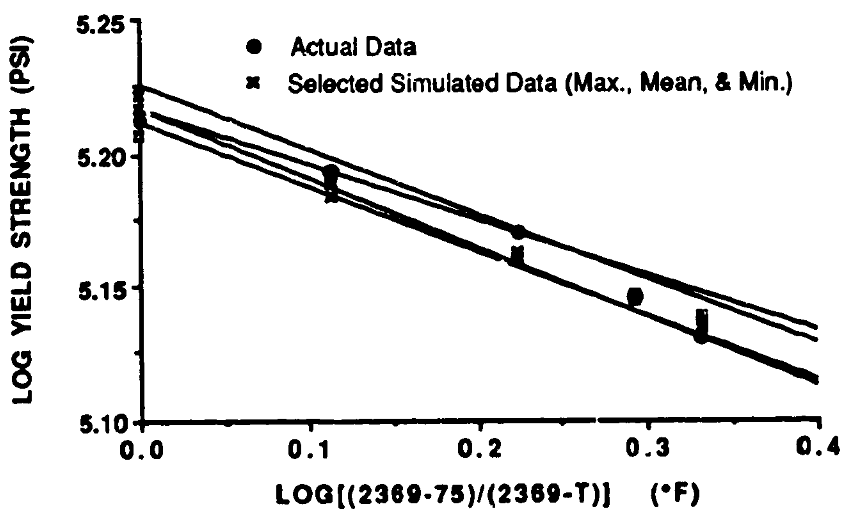

Figure 29 Postulated Envelope of Actual and Simulated Temperature (°F) Data.

7.0 PROBABILISTIC LIFETIME STRENGTH SENSITIVITY STUDIES

7.1 '93 Sensitivity Study for High-Cycle Mechanical Fatigue, Creep and Thermal Fatigue Effects

A modified version of PROMISS, entitled PROMISS93, was developed for sensitizing the model for high-cycle mechanical fatigue, creep and thermal fatigue effects. Using the sensitized probabilistic material strength degradation model embodied in PROMISS93, a lifetime strength sensitivity study was conducted. Three effects were included in this study, high-cycle mechanical fatigue, creep and thermal fatigue. The temperature effect was not explicitly included as a fourth effect since the data used in this study for the other effects resulted from tests conducted at elevated temperatures of 900 to 1000 °F. Therefore, the effect of high temperature is inherent in the high-cycle mechanical fatigue, creep and thermal fatigue empirical material constants used to calibrate the model.

The general form of the multifactor equation given by equation (1), when modified for combined high-cycle mechanical fatigue, creep and thermal fatigue effects, becomes,

$$\frac{S}{S_O}=\left[\frac{N_U-N}{N_U-N_O}\right]^s\left[\frac{t_U-t}{t_U-t_O}\right]^v\left[\frac{N'_U-N'}{N'_U-N'_O}\right]^u \qquad (17a)$$

or

$$\frac{S}{S_O}=\left[\frac{N_U-N_O}{N_U-N}\right]^{-s}\left[\frac{t_U-t_O}{t_U-t}\right]^{-v}\left[\frac{N'_U-N'_O}{N'_U-N'}\right]^{-u}. \qquad (17b)$$

By making the necessary log transformations to increase model sensitivity and accuracy for these three specific effects, equation (17b) becomes,

$$\frac{S}{S_O}=\left[\frac{\log(N_U)-\log(N_O)}{\log(N_U)-\log(N)}\right]^{-s}\left[\frac{\log(t_U)-\log(t_O)}{\log(t_U)-\log(t)}\right]^{-v}\left[\frac{\log(N'_U)-\log(N'_O)}{\log(N'_U)-\log(N')}\right]^{-u}. \qquad (18a)$$

Substitution of the improved ultimate and reference estimates results in equation (18b) below.

$$\frac{S}{S_O}=\left[\frac{\log\left(10^{10}\right)-\log(0.25)}{\log\left(10^{10}\right)-\log(N)}\right]^{-s}\left[\frac{\log\left(10^{5}\right)-\log(0.25)}{\log\left(10^{5}\right)-\log(t)}\right]^{-v}\left[\frac{\log\left(5\times10^{4}\right)-\log(0.25)}{\log\left(5\times10^{4}\right)-\log\left(N'\right)}\right]^{-u} \qquad (18b)$$

The ultimate and reference values in equation (18b) became model parameters or constraints for the multifactor equation when modified for Inconel 718. Figure 30 illustrates these model parameters graphically, wherein each axis represents an effect.

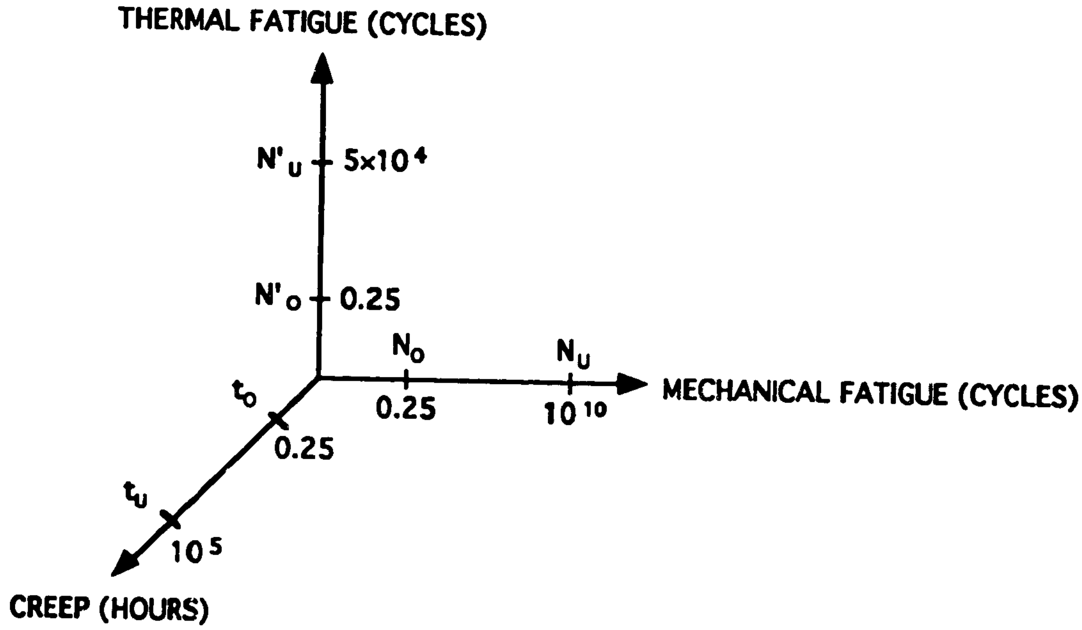

Fig. 30 Inconel 718 Model Parameters for High-Cycle Mechanical Fatigue, Creep and Thermal Fatigue Effects.

Typical sets of input values for the PROMISS model represented by equation (18b) are given in Tables 13, 14 and 15. For example, Table 13 shows PROMISS input data for a temperature of 1000 °F, a current value of $2.5x10^5$ high-cycle mechanical fatigue cycles, a current value of 1000 creep hours, and a current value of 2000 thermal fatigue cycles. As seen in Tables 13 through 15, the above-mentioned current values remain the same with the exception of the current value of high-cycle mechanical fatigue cycles, N. In Tables 14 and 15 the current value of high-cycle mechanical fatigue cycles has been increased to $1.0x10^6$ and $1.75x10^6$, respectively. By holding two of the three sets of current values constant, sensitivity of lifetime strength towards the third set of values, in this case high-cycle mechanical fatigue cycles, can be ascertained. The complete set of current values that were used as input data for this sensitivity study are given in Table 16. Notice that the first three rows of the table correspond to the current values listed in Tables 13, 14 and 15, respectively. The next three rows of Table 16 show how the current values of creep hours were varied, while the last three rows show how the current values of thermal fatigue cycles were varied. The results of this study, in the form of cumulative distribution functions, are given in Figures 31 through 33.

Figure 31 shows the effect of high-cycle mechanical fatigue cycles on lifetime strength, while Figures 32 and 33 show the effect of creep hours and thermal fatigue cycles on lifetime strength, respectively. Note that the c.d.f. shifts to the left, indicating a lowering of lifetime strength, as mechanical fatigue cycles increase. In this manner, results, in the form of c.d.f.'s, display the sensitivity of lifetime strength to any current value of an effect.

Table 13 '93 Sensitivity Study Input to PROMISS93 for Inconel 718; Temperature = 1000 °F and N=2.5x10^5 Cycles.

Effect	Variable Symbol	Units	Distribution Type	Mean	Standard Deviation (Value)	(% of Mean)
High-Cycle Mechanical Fatigue	N_U	cycles	Normal	1.0×10^{10}	1.0×10^{9}	10.0
	N	cycles	Normal	2.5×10^{5}	2.5×10^{4}	10.0
	N_O	cycles	Normal	0.25	0.025	10.0
	s	dimensionless	Normal	0.2235	0.0067	3.0
Creep	t_U	hours	Normal	1.0×10^{5}	1.0×10^{4}	10.0
	t	hours	Normal	1.0×10^{3}	1.0×10^{2}	10.0
	t_O	hours	Normal	0.25	0.025	10.0
	v	dimensionless	Normal	0.1737	0.0052	3.0
Thermal Fatigue	N'_U	cycles	Normal	5.0×10^{4}	5.0×10^{3}	10.0
	N'	cycles	Normal	2.0×10^{3}	2.0×10^{2}	10.0
	N'_O	cycles	Normal	0.25	0.025	10.0
	u	dimensionless	Normal	0.191	0.0057	3.0

Table 14 '93 Sensitivity Study Input to PROMISS93 for Inconel 718; Temperature = 1000 °F and N=1.0x10^6 Cycles.

Effect	Variable Symbol	Units	Distribution Type	Mean	Standard Deviation (Value)	(% of Mean)
High-Cycle Mechanical Fatigue	N_U	cycles	Normal	1.0×10^{10}	1.0×10^{9}	10.0
	N	cycles	Normal	1.0×10^{6}	1.0×10^{5}	10.0
	N_O	cycles	Normal	0.25	0.025	10.0
	s	dimensionless	Normal	0.2235	0.0067	3.0
Creep	t_U	hours	Normal	1.0×10^{5}	1.0×10^{4}	10.0
	t	hours	Normal	1.0×10^{3}	1.0×10^{2}	10.0
	t_O	hours	Normal	0.25	0.025	10.0
	v	dimensionless	Normal	0.1737	0.0052	3.0
Thermal Fatigue	N'_U	cycles	Normal	5.0×10^{4}	5.0×10^{3}	10.0
	N'	cycles	Normal	2.0×10^{3}	2.0×10^{2}	10.0
	N'_O	cycles	Normal	0.25	0.025	10.0
	u	dimensionless	Normal	0.191	0.0057	3.0

Table 15 '93 Sensitivity Study Input to PROMISS93 for Inconel 718; Temperature = 1000 °F and N=1.75×10^6 Cycles

Effect	Variable Symbol	Units	Distribution Type	Mean	Standard Deviation (Value),	(% of Mean)
High-Cycle Mechanical Fatigue	N_U	cycles	Normal	1.0×10^{10}	1.0×10^9	10.0
	N	cycles	Normal	1.75×10^6	1.75×10^5	10.0
	N_O	cycles	Normal	0.25	0.025	10.0
	s	dimensionless	Normal	0.2235	0.0067	3.0
Creep	t_U	hours	Normal	1.0×10^5	1.0×10^4	10.0
	t	hours	Normal	1.0×10^3	1.0×10^2	10.0
	t_O	hours	Normal	0.25	0.025	10.0
	v	dimensionless	Normal	0.1737	0.0052	3.0
Thermal Fatigue	N'_U	cycles	Normal	5.0×10^4	5.0×10^3	10.0
	N'	cycles	Normal	2.0×10^3	2.0×10^2	10.0
	N'_O	cycles	Normal	0.25	0.025	10.0
	u	dimensionless	Normal	0.191	0.0057	3.0

Table 16 Selected Current Values for '93 Sensitivity Study of the Probabilistic Material Strength Degradation Model for Inconel 718.

High-Cycle Mechanical Fatigue (Cycles)	Creep (Hours)	Thermal Fatigue (Cycles)
2.5×10^5	1000	2000
1.0×10^6	1000	2000
1.75×10^6	1000	2000
1.0×10^6	**250**	2000
1.0×10^6	**1000**	2000
1.0×10^6	**1750**	2000
1.0×10^6	1000	**500**
1.0×10^6	1000	**2000**
1.0×10^6	1000	**3500**

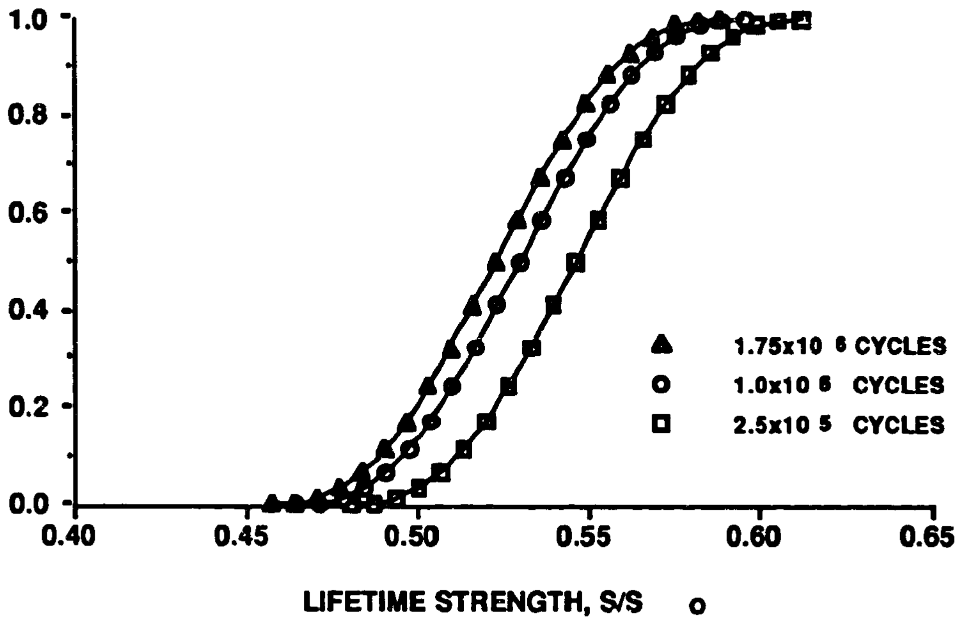

Fig. 31 Comparison of Various Levels of Uncertainty of High-Cycle Mechanical Fatigue (Cycles) on Probable Strength for Inconel 718 for 2000 Thermal Fatigue Cycles and 1000 Hours of Creep at 1000 °F.

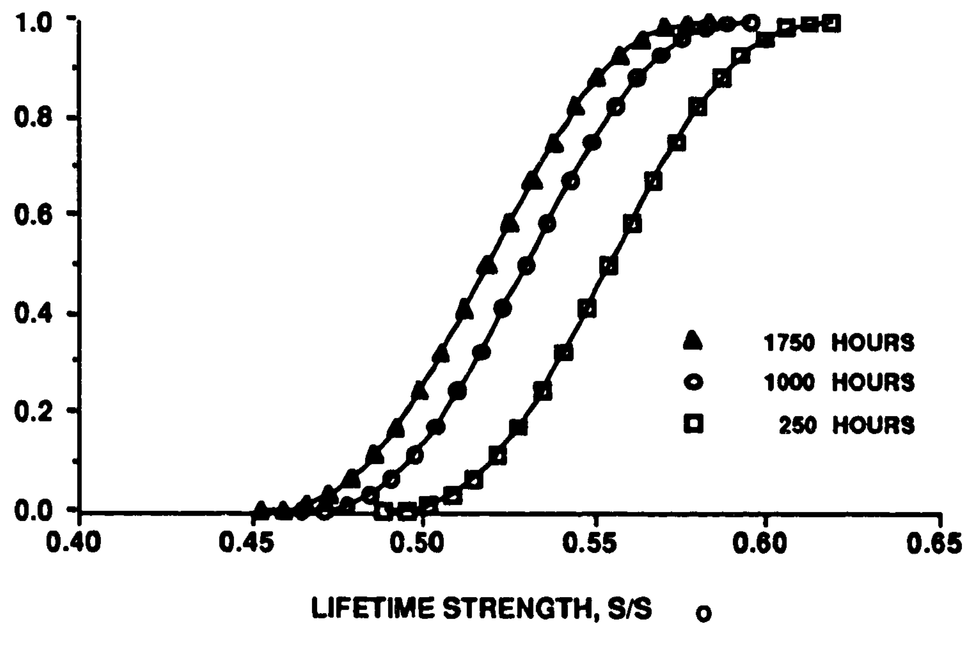

Fig. 32 Comparison of Various Levels of Uncertainty of Creep Time (Hours) on Probable Strength for Inconel 718 for $1x10^6$ High-Cycle Mechanical Fatigue Cycles and 2000 Thermal Fatigue Cycles at 1000 °F.

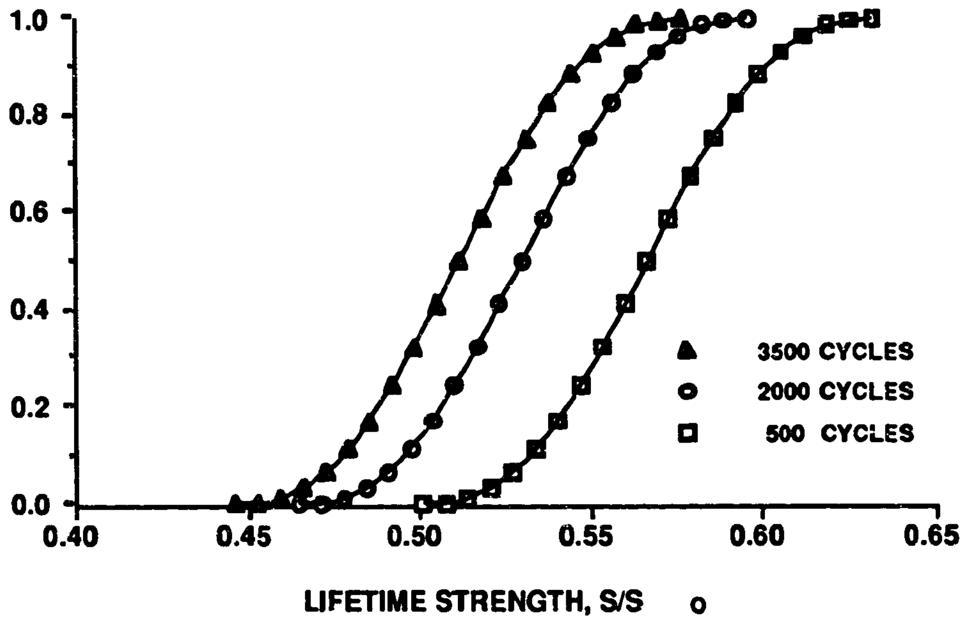

Fig. 33 Comparison of Various Levels of Uncertainty of Thermal Fatigue (Cycles) on Probable Strength for Inconel 718 for 1×10^6 High-Cycle Mechanical Fatigue Cycles and 1000 Hours of Creep at 1000 °F.

7.2 '94 Sensitivity Study for High-Cycle Mechanical Fatigue, Low-Cycle Mechanical Fatigue, Creep and Thermal Fatigue Effects

A modified version of PROMISS93, entitled PROMISS94, was developed for sensitizing the model for yet another effect, low-cycle mechanical fatigue. Using the sensitized probabilistic material strength degradation model embodied in PROMISS94, a second lifetime strength sensitivity study was conducted. Four effects were included in this study, high-cycle mechanical fatigue, low-cycle mechanical fatigue, creep and thermal fatigue. As before, the temperature effect was not explicitly included as a fifth effect since the data used in this study for the other effects resulted from tests conducted at elevated temperatures of 900 to 1000 °F. Therefore, the effect of high temperature is inherent in the high-cycle mechanical fatigue, low-cycle mechanical fatigue, creep and thermal fatigue empirical material constants used to calibrate the model.

The general form of the multifactor equation given by equation (1), when modified for combined high-cycle mechanical fatigue, low-cycle mechanical fatigue, creep and thermal fatigue effects, becomes,

$$\frac{S}{S_O}=\left[\frac{N_U-N}{N_U-N_O}\right]^{s}\left[\frac{N''_U-N''}{N''_U-N''_O}\right]^{r}\left[\frac{t_U-t}{t_U-t_O}\right]^{v}\left[\frac{N'_U-N'}{N'_U-N'_O}\right]^{u} \qquad (19a)$$

or

$$\frac{S}{S_O}=\left[\frac{N_U-N_O}{N_U-N}\right]^{-s}\left[\frac{N''_U-N''_O}{N''_U-N''}\right]^{-r}\left[\frac{t_U-t_O}{t_U-t}\right]^{-v}\left[\frac{N'_U-N'_O}{N'_U-N'}\right]^{-u}. \qquad (19b)$$

By making the necessary log transformations to increase model sensitivity and accuracy for these four specific effects, equation (19b) becomes,

$$\frac{S}{S_O}=\left[\frac{\log(N_U)-\log(N_O)}{\log(N_U)-\log(N)}\right]^{-s}\left[\frac{\log(N''_U)-\log(N''_O)}{\log(N''_U)-\log(N'')}\right]^{-r}\left[\frac{\log(t_U)-\log(t_O)}{\log(t_U)-\log(t)}\right]^{-v}\left[\frac{\log(N'_U)-\log(N'_O)}{\log(N'_U)-\log(N')}\right]^{-u} \qquad (20a)$$

Substitution of the improved ultimate and reference estimates results in equation (20b) below.

$$\frac{S}{S_O}=\left[\frac{\log(10^{10})-\log(0.25)}{\log(10^{10})-\log(N)}\right]^{-s}\left[\frac{\log(5\times10^{4})-\log(0.50)}{\log(5\times10^{4})-\log(N'')}\right]^{-r}\left[\frac{\log(10^{5})-\log(0.25)}{\log(10^{5})-\log(t)}\right]^{-v}\left[\frac{\log(5\times10^{4})-\log(0.25)}{\log(5\times10^{4})-\log(N')}\right]^{-u} \qquad (20b)$$

The complete set of current values that were used as input data for this sensitivity study are given in Table 17. Notice that the first three rows show how the current value of high-cycle mechanical fatigue cycles were varied while the current values for the other three effects were held constant. By holding three of the four sets of current values constant, sensitivity of lifetime strength towards the fourth set of values, in this case high-cycle mechanical fatigue cycles, can be ascertained. The results of this study, in the form of cumulative distribution functions, are given in Figures 34 through 37. Figure 34 shows the effect of high-cycle mechanical fatigue cycles on lifetime strength, while Figures 35, 36 and 37 show the effect of low-cycle mechanical fatigue cycles, creep hours and thermal fatigue cycles on lifetime strength, respectively. As previously shown by the results of the '93 Sensitivity Study, once again the c.d.f. shifts to the left, indicating a lowering of lifetime strength, as high-cycle mechanical fatigue cycles increase. In this manner, results, in the form of c.d.f.'s, display the sensitivity of lifetime strength to any current value of an effect.

Table 17 Selected Current Values for '94 Sensitivity Study of the Probabilistic Material Strength Degradation Model for Inconel 718.

High-Cycle Mechanical Fatigue (Cycles)	Low-Cycle Mechanical Fatigue (Cycles)	Creep (Hours)	Thermal Fatigue (Cycles)
2.5×10^5	1000	1000	2000
1.0×10^6	1000	1000	2000
1.75×10^6	1000	1000	2000
1.0×10^6	**250**	1000	2000
1.0×10^6	**1000**	1000	2000
1.0×10^6	**1750**	1000	2000
1.0×10^6	1000	**250**	2000
1.0×10^6	1000	**1000**	2000
1.0×10^6	1000	**1750**	2000
1.0×10^6	1000	1000	**500**
1.0×10^6	1000	1000	**2000**
1.0×10^6	1000	1000	**3500**

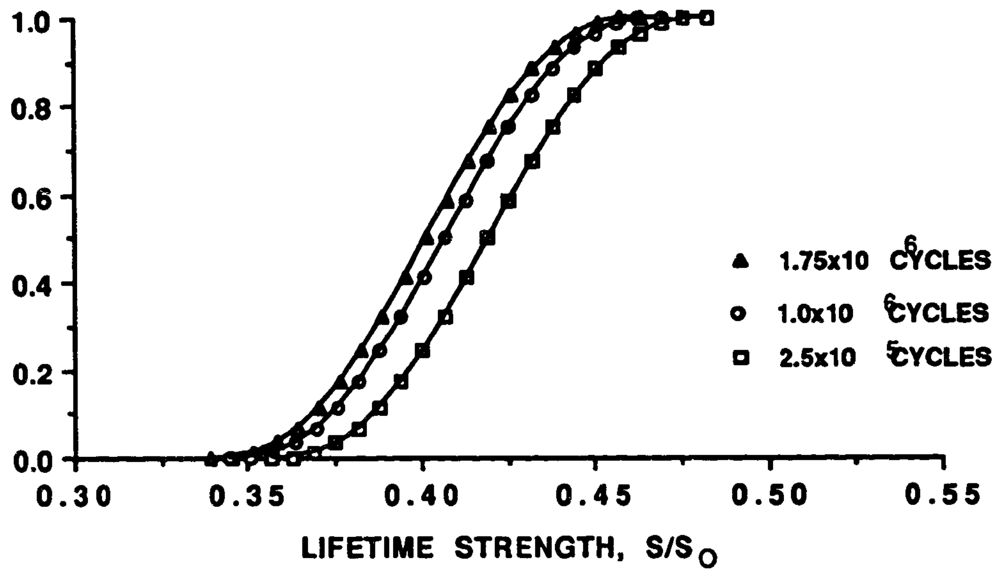

Fig. 34 Comparison of Various Levels of Uncertainty of High-Cycle Mechanical Fatigue (Cycles) on Probable Strength for 1000 Low-Cycle Mechanical Fatigue Cycles, 2000 Thermal Fatigue Cycles and 1000 Hours of Creep at 1000 °F.

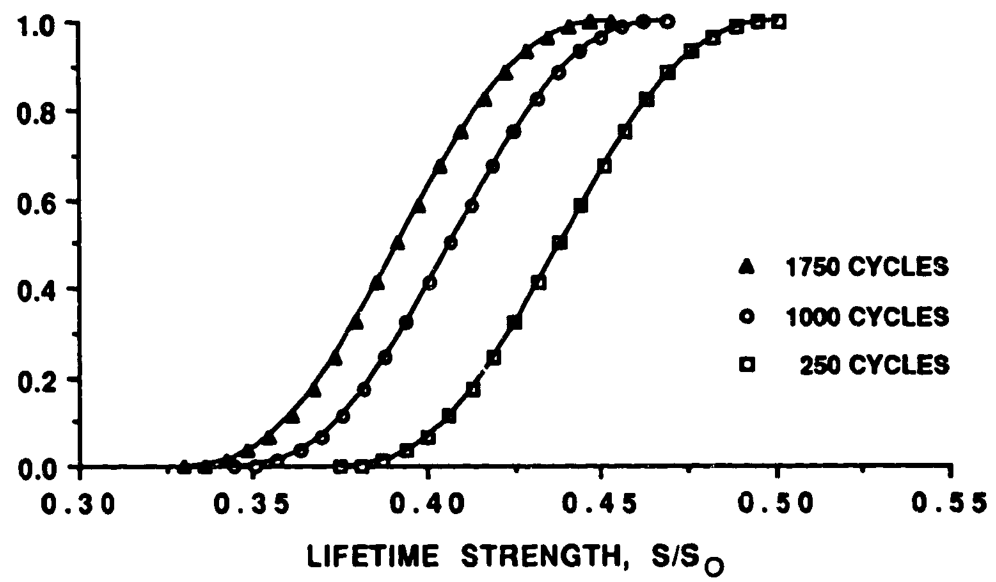

Fig. 35 Comparison of Various Levels of Uncertainty of Low-Cycle Mechanical Fatigue (Cycles) on Probable Strength for 1×10^6 High-Cycle Mechanical Fatigue Cycles, 2000 Thermal Fatigue Cycles and 1000 Hours of Creep at 1000 °F.

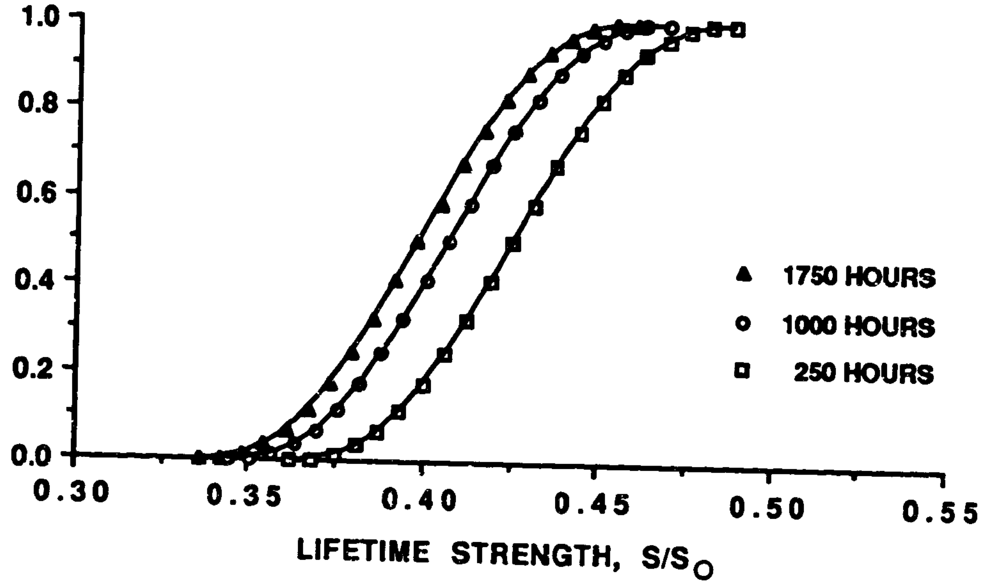

Fig. 36 Comparison of Various Levels of Uncertainty of Creep Time (Hours) on Probable Strength for 1×10^6 High-Cycle Mechanical Fatigue Cycles, 1000 Low-Cycle Mechanical Fatigue Cycles and 2000 Thermal Fatigue Cycles at 1000 °F.

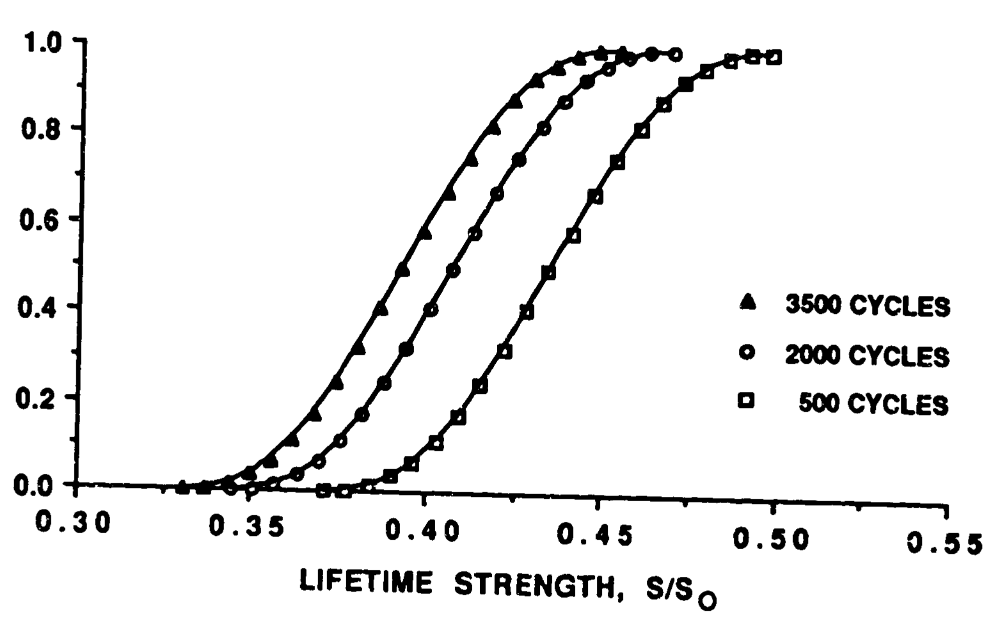

Fig. 37 Comparison of Various Levels of Uncertainty of Thermal Fatigue (Cycles) on Probable Strength for 1×10^6 High-Cycle Mechanical Fatigue Cycles, 1000 Low-Cycle Mechanical Fatigue Cycles and 1000 Hours of Creep at 1000 °F.

8.0 MODEL VERIFICATION STUDY

Using the probabilistic material strength degradation model embodied in PROMISS, a model verification study was conducted. The basic assumption, that two or more effects acting on the material multiply (i.e., independent variables), was evaluated. Available data allowed for a verification study comparing a combination of high-cycle mechanical fatigue effects at 75 °F and temperature effects at 1000 °F to high-cycle mechanical fatigue effects at 1000 °F. That is, a combination of high-cycle mechanical fatigue and temperature by model was compared to the combination of these two effects by experiment. The input values for the combination of these two effects by model are given in Tables 18 through 20, while the input values for the combination of these two effects by experiment are provided in Tables 21 through 23. Three different current values of high-cycle mechanical fatigue cycles were used so that the verification study would encompass a range of fatigue cycle values. The results of this study, in the form of cumulative distribution functions, are given in Figures 38 through 40. Figure 38 displays lifetime strength predictions for the combination of high-cycle mechanical fatigue and temperature by model, while Figure 39 displays results for the combination of these two effects by experiment. Figure 40 is an overlay of the two sets of results. It is evident that there is approximately a 20% difference between the two sets of distributions.

Due to the questionable high-cycle mechanical fatigue material constant (s = 0.37848) used in the combination by model input, a second verification study was conducted. Once again, a combination of these two effects by model was compared to the combination by experiment. However, an adjusted high-cycle mechanical fatigue material constant (s = 0.141) was input in place of the questionable high-cycle mechanical fatigue material constant at a temperature of 75 °F. This value was estimated by noting the percent difference (37 %) between the calculated slopes at 1000 °F and 1200 °F. The improved input values for this second verification study are provided in Tables 24 through 26. The input values for combination by experiment were the same as before. The results are given by Figures 41 through 44. Figure 41, overlays the results for the combination by model and those by experiment. The 20% difference was greatly reduced. For clarity, Figures 42, 43 and 44 overlay the results for both model and experiment for current mechanical fatigue cycle values of 2.5×10^5, 1×10^6 and 1.75×10^6 cycles, respectively. A percent difference of less than 5% was observed for all three current mechanical fatigue cycle values.

Table 18 Verification Study Input to PROMISS93 for Inconel 718; Combination by Model, $N=2.5\times10^5$ cycles.

Effect	Variable Symbol	Units	Distribution Type	Mean	Standard Deviation (Value)	(% of Mean)
High-Cycle	N_U	cycle	Normal	1.0×10^{10}	1.0×10^9	10.0
Mechanical	N	cycle	Normal	2.5×10^5	2.5×10^4	10.0
Fatigue	N_O	cycle	Normal	0.25	0.025	10.0
(at 75 °F)	s	dimensionless	Normal	0.3785	0.0114	3.0
High	T_U	°F	Normal	2369.0	236.90	10.0
Temperature	T	°F	Normal	1000.0	100.00	10.0
(at 1000 °F)	T_O	°F	Normal	75.0	7.50	10.0
	q	dimensionless	Normal	0.2422	0.0088	3.6

Table 19 Verification Study Input to PROMISS93 for Inconel 718; Combination by Model, $N=1.0\times10^6$ cycles.

Effect	Variable Symbol	Units	Distribution Type	Mean	Standard Deviation (Value)	(% of Mean)
High-Cycle	N_U	cycle	Normal	1.0×10^{10}	1.0×10^9	10.0
Mechanical	N	cycle	Normal	1.0×10^6	1.0×10^5	10.0
Fatigue	N_O	cycle	Normal	0.25	0.025	10.0
(at 75 °F)	s	dimensionless	Normal	0.3785	0.0114	3.0
High	T_U	°F	Normal	2369.0	236.90	10.0
Temperature	T	°F	Normal	1000.0	100.00	10.0
(at 1000 °F)	T_O	°F	Normal	75.0	7.50	10.0
	q	dimensionless	Normal	0.2422	0.0088	3.6

Table 20 Verification Study Input to PROMISS93 for Inconel 718; Combination by Model, $N=1.75\times10^6$ cycles.

Effect	Variable Symbol	Units	Distribution Type	Mean	Standard Deviation (Value)	(% of Mean)
High-Cycle	N_U	cycle	Normal	1.0×10^{10}	1.0×10^9	10.0
Mechanical	N	cycle	Normal	1.75×10^6	1.75×10^5	10.0
Fatigue	N_O	cycle	Normal	0.25	0.025	10.0
(at 75 °F)	s	dimensionless	Normal	0.3785	0.0114	3.0
High	T_U	°F	Normal	2369.0	236.90	10.0
Temperature	T	°F	Normal	1000.0	100.00	10.0
(at 1000 °F)	T_O	°F	Normal	75.0	7.50	10.0
	q	dimensionless	Normal	0.2422	0.0088	3.6

Table 21 Verification Study Input to PROMISS93 for Inconel 718; Combination by Experiment, $N=2.5\times10^5$ cycles.

Effect	Variable Symbol	Units	Distribution Type	Mean	Standard Deviation (Value),	(% of Mean)
High-Cycle	N_U	cycle	Normal	1.0×10^{10}	1.0×10^9	10.0
Mechanical	N	cycle	Normal	2.5×10^5	2.5×10^4	10.0
Fatigue	N_O	cycle	Normal	0.25	0.025	10.0
(at 1000 °F)	s	dimensionless	Normal	0.2235	0.0067	3.0

Table 22 Verification Study Input to PROMISS93 for Inconel 718; Combination by Experiment, $N=1.0\times10^6$ cycles.

Effect	Variable Symbol	Units	Distribution Type	Mean	Standard Deviation (Value),	(% of Mean)
High-Cycle	N_U	cycle	Normal	1.0×10^{10}	1.0×10^9	10.0
Mechanical	N	cycle	Normal	1.0×10^6	1.0×10^5	10.0
Fatigue	N_O	cycle	Normal	0.25	0.025	10.0
(at 1000 °F)	s	dimensionless	Normal	0.2235	0.0067	3.0

Table 23 Verification Study Input to PROMISS93 for Inconel 718; Combination by Experiment, $N=1.75\times10^6$ cycles.

Effect	Variable Symbol	Units	Distribution Type	Mean	Standard Deviation (Value),	(% of Mean)
High-Cycle	N_U	cycle	Normal	1.0×10^{10}	1.0×10^9	10.0
Mechanical	N	cycle	Normal	1.75×10^6	1.75×10^5	10.0
Fatigue	N_O	cycle	Normal	0.25	0.025	10.0
(at 1000 °F)	s	dimensionless	Normal	0.2235	0.0067	3.0

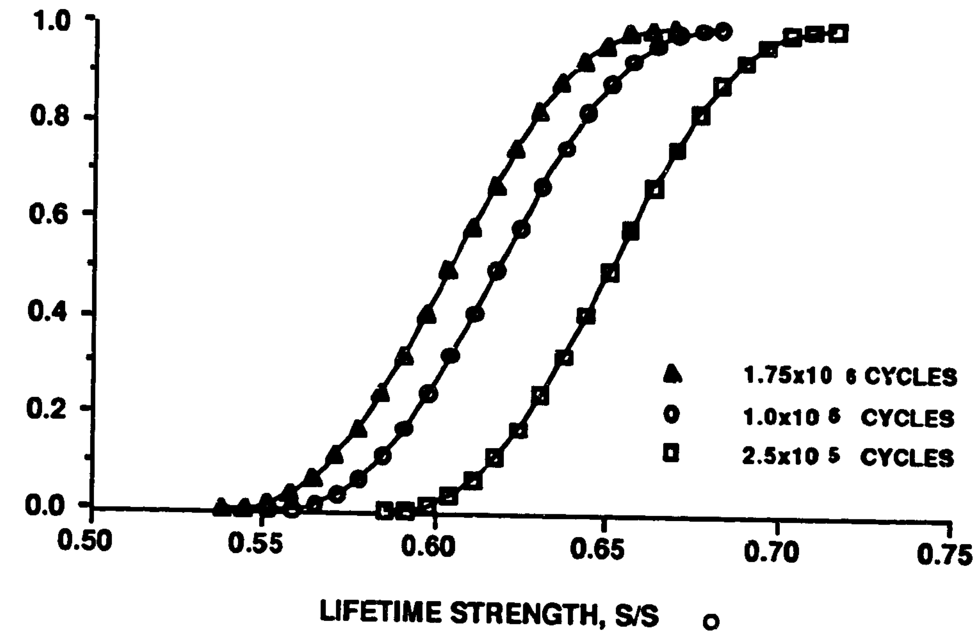

Figure 38 Comparison of Various Levels of Uncertainty of High-Cycle Mechanical Fatigue (Cycles) on Probable Strength for Inconel 718.
(Combination of H-C Mechanical Fatigue and High Temperature Effects by Model)

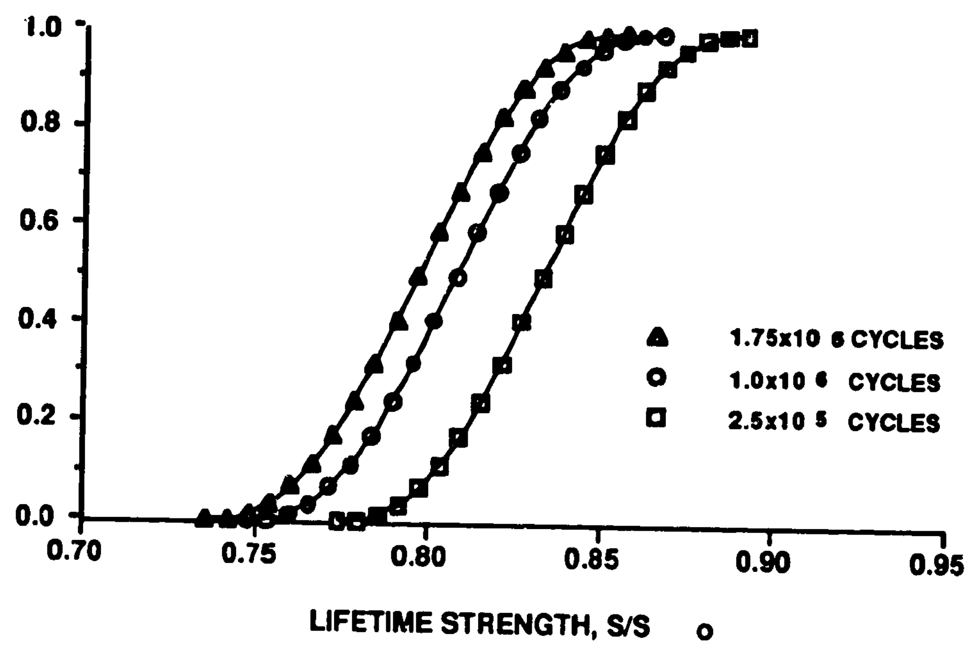

Figure 39 Comparison of Various Levels of Uncertainty of High-Cycle Mechanical Fatigue (Cycles) on Probable Strength for Inconel 718.
(Combination of H-C Mechanical Fatigue and High Temperature Effects by Experiment)

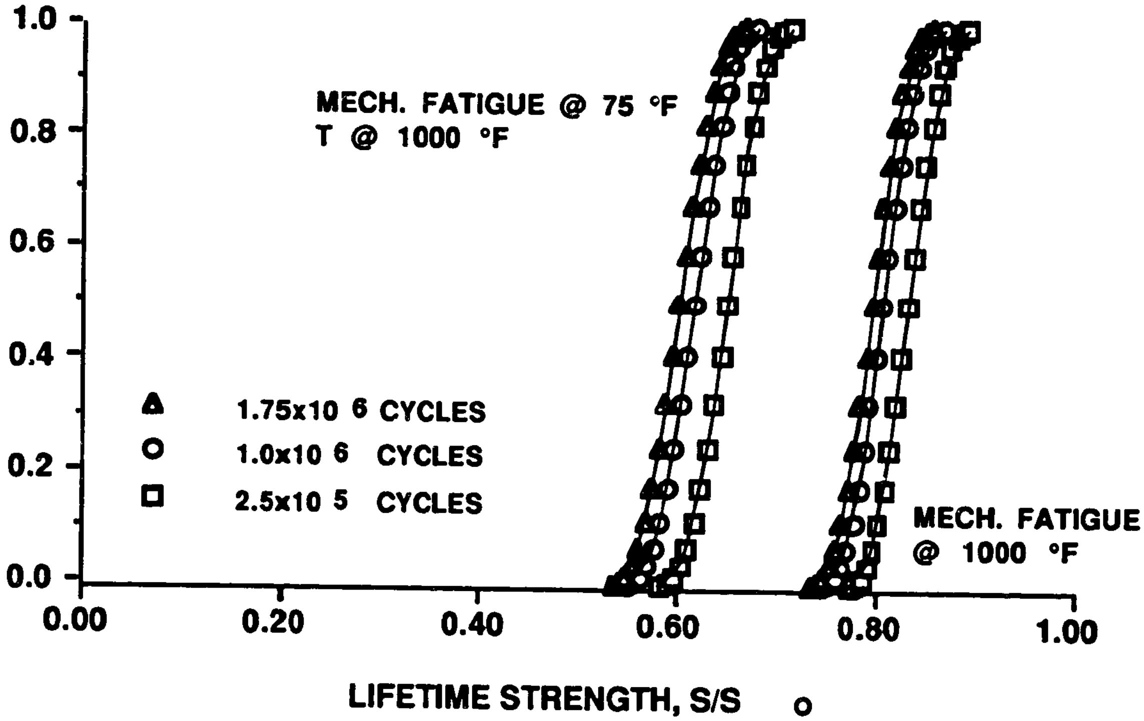

Figure 40 Overlay of Results for the Combination of High-Cycle Mechanical Fatigue and Temperature Effects by Model and Experiment.

Table 24 Modified Verification Study Input to PROMISS93 for Inconel 718; Combination by Model, N=2.5x10^5 cycles.

Effect	Variable Symbol	Units	Distribution Type	Mean	Standard Deviation (Value)	(% of Mean)
High-Cycle	N_U	cycle	Normal	1.0x10^{10}	1.0x10^9	10.0
Mechanical	N	cycle	Normal	2.5x10^5	2.5x10^4	10.0
Fatigue	N_O	cycle	Normal	0.25	0.025	10.0
(at 75 °F)	s	dimensionless	Normal	0.141	0.0042	3.0
High	T_U	°F	Normal	2369.0	236.90	10.0
Temperature	T	°F	Normal	1000.0	100.00	10.0
(at 1000 °F)	T_O	°F	Normal	75.0	7.50	10.0
	q	dimensionless	Normal	0.2422	0.0088	3.6

Table 25 Modified Verification Study Input to PROMISS93 for Inconel 718; Combination by Model, N=1.0x10^6 cycles.

Effect	Variable Symbol	Units	Distribution Type	Mean	Standard Deviation (Value)	(% of Mean)
High-Cycle	N_U	cycle	Normal	1.0x10^{10}	1.0x10^9	10.0
Mechanical	N	cycle	Normal	1.0x10^6	1.0x10^5	10.0
Fatigue	N_O	cycle	Normal	0.25	0.025	10.0
(at 75 °F)	s	dimensionless	Normal	0.141	0.0042	3.0
High	T_U	°F	Normal	2369.0	236.90	10.0
Temperature	T	°F	Normal	1000.0	100.00	10.0
(at 1000 °F)	T_O	°F	Normal	75.0	7.50	10.0
	q	dimensionless	Normal	0.2422	0.0088	3.6

Table 26 Modified Verification Study Input to PROMISS93 for Inconel 718; Combination by Model, N=1.75x10^6 cycles.

Effect	Variable Symbol	Units	Distribution Type	Mean	Standard Deviation (Value)	(% of Mean)
High-Cycle	N_U	cycle	Normal	1.0x10^{10}	1.0x10^9	10.0
Mechanical	N	cycle	Normal	1.75x10^6	1.75x10^5	10.0
Fatigue	N_O	cycle	Normal	0.25	0.025	10.0
(at 75 °F)	s	dimensionless	Normal	0.141	0.0042	3.0
High	T_U	°F	Normal	2369.0	236.90	10.0
Temperature	T	°F	Normal	1000.0	100.00	10.0
(at 1000 °F)	T_O	°F	Normal	75.0	7.50	10.0
	q	dimensionless	Normal	0.2422	0.0088	3.6

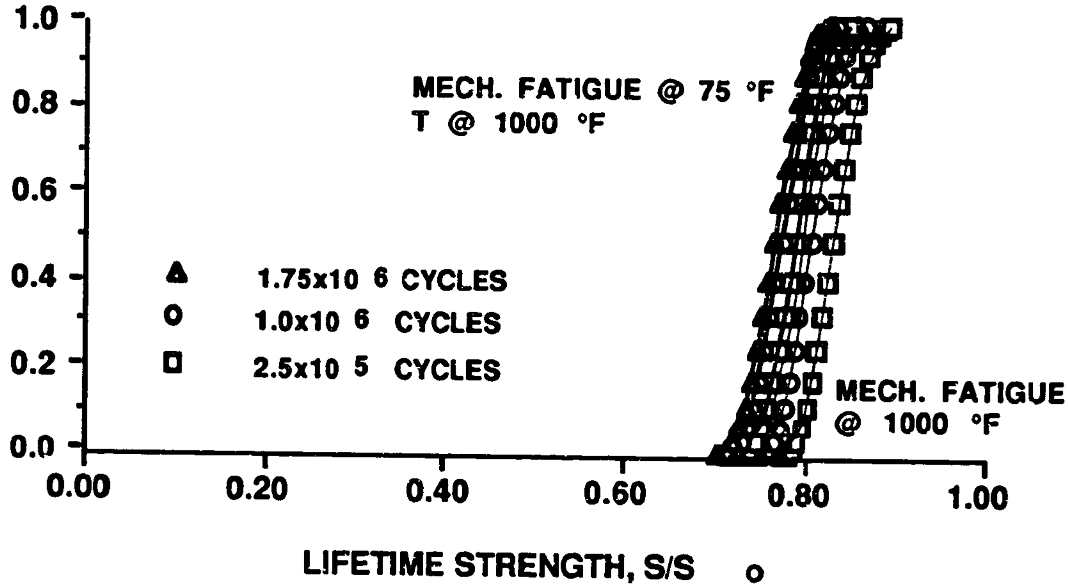

Figure 41 Overlay of Results for the Combination of High-Cycle Mechanical Fatigue and Temperature Effects by Model (Using Estimated Value of s) and Experiment.

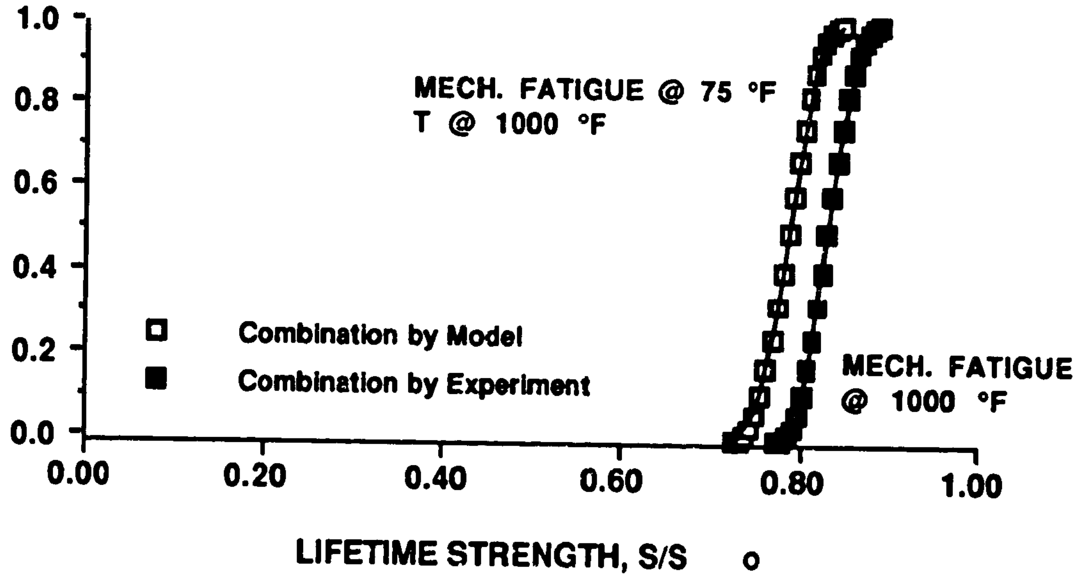

Figure 42 Overlay of Results for the Combination of High-Cycle Mechanical Fatigue and Temperature Effects by Model (Using Estimated Value of s) and Experiment; $N=2.5\times10^5$ Cycles.

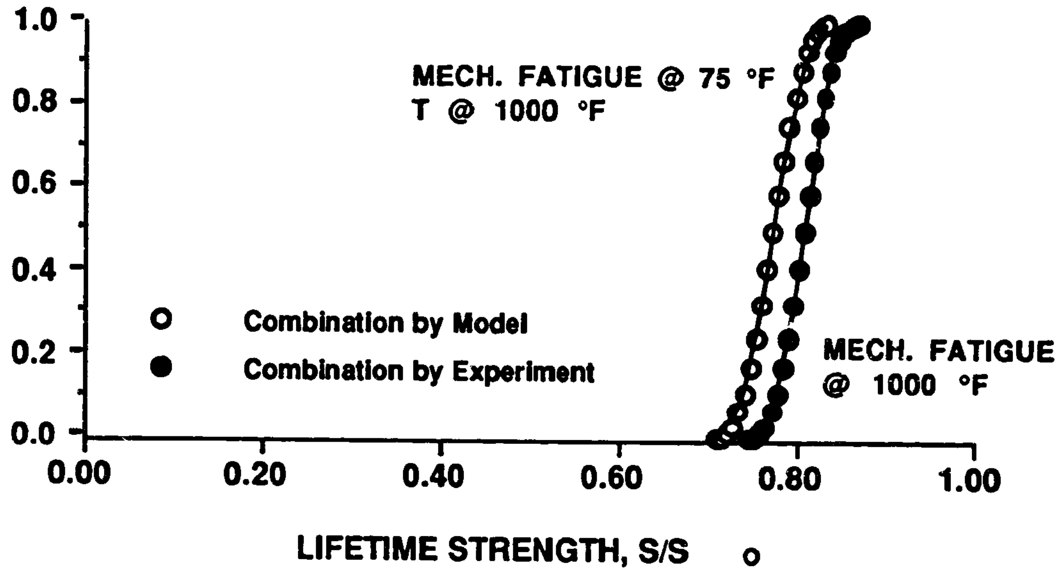

Figure 43 Overlay of Results for the Combination of High-Cycle Mechanical Fatigue and Temperature Effects by Model (Using Estimated Value of s) and Experiment; $N=1.0\times10^6$ Cycles.

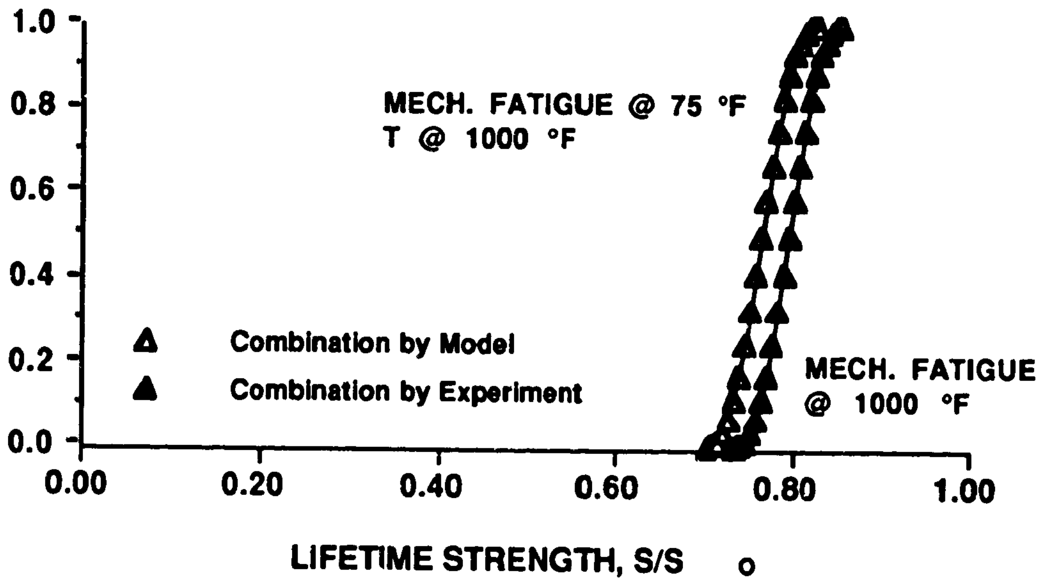

Figure 44 Overlay of Results for the Combination of High-Cycle Mechanical Fatigue and Temperature Effects by Model (Using Estimated Value of s) and Experiment; $N=1.75\times10^6$ Cycles.

9.0 DISCUSSION

To ensure model accuracy in lifetime strength predictions, close attention was paid to model sensitization and calibration. When the current value and the reference value were small compared to the ultimate value, model transformation, by taking the log of each value within the product term, was required for model sensitivity. As shown for high-cycle mechanical fatigue, low-cycle mechanical fatigue, creep and thermal fatigue effects in Figures 5 through 6, 8 through 9, 11 through 12, and 19 through 20, respectively, this transformation resulted in considerable increases in the linear regression R^2 values. The closer the R^2 value is to a value of one, the better the linear regression fit.

Calibration of the model specifically for Inconel 718 required actual experimental data. Based on this data, initial ultimate and reference values for each effect were estimated and are provided in Table 9. Linear regression of data individually for each effect resulted in initial estimates for the empirical material constants. These constants for temperature, high-cycle mechanical fatigue, low-cycle mechanical fatigue, creep and thermal fatigue effects are given in Table 10. Further calibration involved adjusting these initial estimates so that y-intercept ($\log S_O$) values, resulting from linear regression analysis, corresponded to average yield strength values of Inconel 718 at specified temperatures. By correlating the S_O values for all effects to average yield strengths, accuracy in modeling two or more effects was increased. These improved estimates are given in Tables 11 and 12. These estimates were used for the mean values in sensitivity study input files (Tables 13 through 15) to PROMISS93 and PROMISS94.

Methodology for estimating the variability of the empirical material constants was developed in Section 6 as a means for dealing with limited data. For the temperature effect, a standard deviation value of 0.0088 or 3.6% of the mean slope (0.2422) was calculated. This value, rather than expert opinion, may be used with greater confidence in the probabilistic material strength degradation model embodied in PROMISS94. Parallel steps may be taken to determine standard deviation estimates for the empirical material constants of the other effects.

The first sensitivity study ('93 Sensitivity Study), discussed in Section 7.0, included only three effects, high-cycle mechanical fatigue, creep and thermal fatigue, as modeled by equation (18b). The results of this study, in the form of cumulative distribution functions, are given in Figures 31 through 33. The sensitivity of lifetime strength to the number of high-cycle mechanical fatigue cycles is seen by the shift of the c.d.f. to the left in Figure 31 as the number of cycles increases from 2.5×10^5 to 1.75×10^6. The same phenomenon is seen in Figures 32 and 33. Thus, increasing the current number of the variable decreased the predicted lifetime strength as expected. The temperature effect was not explicitly included in this study due to the fact that data for the other three effects resulted from tests conducted in a high temperature environment (900 °F to 1000 °F). Thus, the effect of temperature is inherent in the estimated empirical material constants for the other three effects. This is evidenced by the changing slopes in Figure 23 for the creep effect. The slope or material constant changes according to the test temperature. At a test temperature of 1000 °F, the material constant (slope) is -0.17372, but increases with temperature to a "steeper" value of -0.75557 at a test temperature of 1300 °F. An increase in the material constant with an increase in temperature is expected. However, as seen by Figure 21, the high-cycle mechanical fatigue material constant (slope) is highest at the lowest test temperature of 75 °F. Since this slope is based upon only four questionable data points, it is presumed to be inaccurate. Therefore, based on observed trends in the change of slopes for the high-cycle mechanical fatigue effect at temperatures of 1000 °F and 1200 °F (Figure 21), an adjusted value for the high-cycle mechanical fatigue material constant at 75 °F was determined. The result was a modified slope 37% less than the slope obtained at a temperature of 1000 °F. Without additional high-cycle mechanical fatigue data at a test temperature of 75 °F, this adjusted slope can be neither confirmed nor rejected.

A second sensitivity study ('94 Sensitivity Study), discussed in Section 7.0, included four effects, high-cycle mechanical fatigue, low-cycle mechanical fatigue, creep and thermal fatigue, as modeled by equation (20b). The results of this study, in the form of cumulative distribution functions, are given in Figures 34 through 37. The sensitivity of lifetime strength to the number of high-cycle mechanical fatigue cycles is seen by the shift of the c.d.f. to the left in Figure 34 as the number of cycles increases from 2.5×10^5 to 1.75×10^6. The same phenomenon is seen in Figures 35 through 37. Thus, increasing the current number of the variable decreased the predicted lifetime strength as expected. As with the '93 Sensitivity Study, the temperature effect was not explicitly included in the '94 Sensitivity Study since it is inherent in the estimated empirical material constants for the other four effects. Comparison of results between the '94 Sensitivity Study and the '93 Sensitivity Study, show a reduction in Lifetime Strength, S/S_0. This was expected since each effect contributes to the decrease in the lifetime strength of the material. Thus, lifetime strength values resulting from a study including four effects will be lower than values resulting from a study including only three effects.

Both the questionable (s = 0.37848) and the adjusted (s = 0.141) high-cycle mechanical fatigue material constants at 75 °F were used in verification studies presented in Section 8. Available data allowed for a verification study comparing a combination of high-cycle mechanical fatigue and temperature effects by model to the combination of these two effects by experiment. The results of this study, in the form of c.d.f.'s, are given in Figures 38 through 40. The sensitivity of lifetime strength to the number of current mechanical fatigue cycles is seen by the shift of the c.d.f. to the left (Figures 38 and 39) as the number of cycles increases. Thus, increasing the number of current fatigue cycles decreases the predicted lifetime strength as expected. As seen by the overlay of distributions in Figure 40, there is approximately a 20% difference between the results obtained by model and those obtained by experiment. A major possibility for this large discrepancy is the questionable high-cycle mechanical fatigue material constant at 75 °F. To test this assumption, a second parallel verification study using the adjusted high-cycle mechanical fatigue material constant value was conducted. The results are given in Figures 41 through 44. Comparison of Figure 41 to Figure 40 shows a substantial decrease in the discrepancy between the two sets of distributions. From Figures 42 through 44, it is apparent that the percent difference between the results is less than 5% for all three current values of fatigue cycles evaluated. Thus, the questionable high-cycle mechanical fatigue material constant calculated from the high-cycle mechanical fatigue data at 75 °F was responsible for a large percent of the discrepancy between the initial results from the first verification study.

10.0 CONCLUSIONS

A probabilistic material strength degradation model, applicable to aerospace materials, has been postulated for predicting the random lifetime strength of structural components for propulsion system components subjected to a number of effects. This model, in the form of a randomized multifactor equation, has been developed for five effects, namely, high temperature, high-cycle mechanical fatigue, low-cycle mechanical fatigue, creep and thermal fatigue. Inconel 718 data for these effects was obtained from the open literature. Based on this data, initial ultimate and reference values were estimated. It was determined that when the current and reference values are small compared to the ultimate value the model is insensitive. Therefore, a transformation to sensitize the model for the effects of high-cycle and low-cycle mechanical fatigue, creep and thermal fatigue was required. Model transformation resulted in significant increases in the R^2 (goodness of fit) values. The current version of PROMISS, entitled PROMISS94, provides for this transformation for these four effects.

Linear regression of the data for each effect resulted in estimates for the empirical material constants, as given by the slope of the linear fit. These estimates, together with ultimate and reference values, were used to calibrate the model specifically for Inconel 718. By adjusting these initial estimates so that the y-intercept or S_O values corresponded to average yield strength values of Inconel 718, accuracy in modeling two or more effects was improved. Thus, model accuracy is dependent on the proper selection of ultimate and reference values, which in turn influence the values of the empirical material constants used in calibration of the model. Calibration of the model for other materials is also dependent on experimental data and is not possible without it.

Methodology for estimating the standard deviation of empirical material constants offered a way for dealing with limited data. This methodology results in better estimates of the standard deviations based on actual experimental data, rather than expert opinion. Lack of sufficient data from which to evaluate the material constants warranted the development of this methodology.

Results from two separate sensitivity studies involving three and four effects, respectively, showed that the c.d.f.'s shift to the left, indicating a lowering of lifetime strength, for increasing current values of an effect. As expected, comparison between the '94 Sensitivity Study and the '93 Sensitivity Study revealed a reduction in the lifetime strength values. Thus, the more effects included in a study, the lower the resulting lifetime strength values. Further development and evaluation of the three and four effect models, as well as other models, requires that they be compared to real responses of Inconel 718 samples subjected to the same combined effects during experimentation. Thus, additional experimental data is crucial for the continued development and evaluation of the probabilistic material strength degradation model presented in this report.

Limited verification studies involving two effects, high-cycle mechanical fatigue and high temperature, were conducted. Results showed a combination of the two effects by model to be more conservative than the combination by experiment. The first verification study yielded a 20% discrepancy between the results obtained by model and those obtained by experiment. Questionable high-cycle mechanical fatigue data at a temperature of 75 °F is presumed to be a major cause of the discrepancy. This conclusion was drawn after conducting a second verification study using an adjusted value in place of the questionable one. The outcome was a significant reduction in the discrepancy, from 20% to less than 5%, between the results of a combination of these two effects by model and the combination by experiment. Therefore, the data, rather than the nature of the model, is the presumed source of error. Thus, the basic assumption of the model, that two or more effects multiply (i.e., effects are independent), is strongly supported by this limited verification study. The remaining 5% difference may be due to the lack of uniformity among the specimens tested. As seen by Table A.5 in the Appendix, specimen shape and heat treatment varied between the effects. Specimen shape, as well as heat treatment, can influence material properties. Another reason for the 5% difference may be synergistic effects (i.e., dependence between effects). As previously discussed, equation (1) is an approximated solution to a separable partial differential equation. In order to account for synergistic effects and perhaps eliminate this 5% difference, additional terms would have to be added to equation (1). The resulting reduction in error may or may not warrant complication of the model by the inclusion of additional terms. Based on the results obtained from the second verification study, this complication is not warranted. However, additional verification studies for the combination of other effects must first be conducted before a more refined model can be developed. As previously discussed, the availability of experimental data will determine whether or not further studies can be conducted.

In conclusion, methodology for improving lifetime strength prediction capabilities is presented. The probabilistic material strength degradation model in the form of a randomized multifactor equation is developed for five effects and calibrated to best reflect physical reality for Inconel 718. Systematic and repeatable methods of model calibration and evaluation are developed. Basic understanding and evaluation of the model is generated through sensitivity and verification studies. The sensitivity of random lifetime strength to any current value of an effect can be ascertained. Probability statements in the form of cumulative distribution functions allow improved judgments to be made regarding the likelihood of lifetime strength, thus enabling better design decisions to be made.

11.0 ACKNOWLEDGMENTS

The authors gratefully acknowledge the many helpful conversations with Dr. Christos C. Chamis and the support of NASA Lewis Research Center.

12.0 APPENDIX

This appendix provides the experimental Inconel 718 data analyzed by the postulated material strength degradation model. The purpose of this appendix is to allow the calculations of Section 5 to be repeated. Data for all effects will be presented in tabular form. Tables A.1-A.5 present the high temperature, high-cycle mechanical fatigue, low-cycle mechanical fatigue, thermal fatigue and creep data, respectively. Table A.6 provides reference numbers and figure numbers for displayed data, as well as, specimen and heat treatment specifications for all data presented in this report.

Table A.1 Inconel 718 High Temperature Tensile Data.

TEST TEMPERATURE, °F	TENSILE STRENGTH, PSI
7.50E+01	1.63E+05
6.00E+02	1.56E+05
1.00E+03	1.48E+05
1.20E+03	1.40E+05
1.30E+03	1.35E+05

Table A.2 Inconel 718 High-Cycle Mechanical Fatigue Data.

TEST TEMPERATURE, °F	FATIGUE STRENGTH, PSI			
	10^5 CYCLES	10^6 CYCLES	10^7 CYCLES	10^8 CYCLES
75	132,000	101,000	92,000	90,000
1000	111,000	102,000	95,000	90,000
1200	100,000	94,000	88,000	72,000

Table A.3 Inconel 718 Low-Cycle Mechanical Fatigue Data.

Test Temperature, °F	Cycles to Failure N''_F	Elastic Strain, $\Delta\varepsilon_e$ %	Plastic Strain, $\Delta\varepsilon_p$ %
1000	2×10^2	1.35	2.80
	4×10^2	1.25	1.85
	6×10^2	1.20	1.50
	8×10^2	1.15	1.20
	1×10^3	1.10	1.00
	2×10^3	1.05	0.68
	4×10^3	1.00	0.42
	6×10^3	0.95	0.36
	8×10^3	0.92	0.30
	1×10^4	0.90	0.26
	2×10^4	0.85	0.17

Table A.4 Inconel 718 Thermal Fatigue Data.

Cycles to Failure, N'_F	Reversals to Failure, $2N'_F$	Total Strain Amplitude	Plastic Strain Amplitude
45	90	0.01	0.005
140	280	0.0075	0.0029
750	1500	0.005	0.0011
9750	19500	0.004	0.0003

Table A.5 Inconel 718 Creep Rupture Data.

TEST TEMPERATURE, °F	RUPTURE LIFE, HRS	RUPTURE STRENGTH, PSI
1000	27.8	158000
	133.2	150000
	256.0	145000
	814.9	140000
	1731.0	134000
	8473.0	124000
	21523.6	118000
1100	28.2	135000
	62.0	130000
	151.9	123000
	367.5	117000
	2327.6	105000
	10606.2	94000
	33990.7	86000
1200	10.6	115000
	30.8	108000
	150.0	96000
	747.2	87000
	3131.5	78000
	7263.0	68000
	10232.0	63000
1300	18.0	86000
	70.5	76000
	182.7	68000
	476.8	60000
	808.0	55000
	2870.7	44000
	6048.0	37000

Table A.6 Inconel 718 Data Summary.

EFFECT	REFERENCE NUMBER	FIGURE NUMBER	SPECIMEN	HEAT TREATMENT
Temperature	[15]	2, 3, 25, 26, 27, 29	hot-rolled round, 4-inch diameter, from single sheet	1950°F/1 hr, plus 1400°F/10 hr, F.C. 100 °F/hr to 1200°F, hold at 1200°F for 8 hr
High-Cycle Mechanical Fatigue	[15]	4, 5, 6, 21	forging, hot-rolled bar, average grain size of 0.0008 in	1750°F/1 hr, plus 1325°F/8 hr, F.C. to 1150°F, hold at 1150°F, total aging time of 18 hr
Low-Cycle Mechanical Fatigue	[7]	7, 8, 9, 22		940 C solution anneal, plus aging
Creep	[2]	10, 11, 12, 23	flat-pancake, 21 in diameter × 1 in thick	1800°F/2 hr, A.C., plus 1325°F/8 hr, F.C. 100°F/hr to 1150°F/8 hr, A.C.
Thermal Fatigue	[17]	13, 14, 15, 16, 17, 18, 19, 20, 24	forging, round, 11 mm diameter, gage length of 15 mm	1253K × 1 hr, W.Q., 997K × 8 hr -(55K/hr) to 893K × 8 hr, A.C.

13.0 REFERENCES

1 Bannantine, J. A., et. al., Fundamentals of Metal Fatigue Analysis, Prentice Hall, Englewood Cliffs, N.J., 1990, pp. 63 - 66.

2 Barker, J. F., Ross, E.W. and Radavich, J. F., "Long Time Stability of INCONEL 718," Journal of Metals, Jan. 1970, Vol. 22, p. 32.

3 Blank, L. T., Statistical Procedures for Engineering, Management and Science, McGraw-Hill, N. Y., 1980, pp. 518, 523.

4 Boyce L. and Bast C., "Computational Simulation of Coupled Material Degradation Processes for Probabilistic Lifetime Strength of Aerospace Materials," NASA CR 1887234, NASA Lewis Research Center, Cleveland, Ohio, March 1992.

5 Boyce, L. and Chamis, C. C., "Probabilistic Constitutive Relationships for Material Strength Degradation Models," Proceedings of the 30th Structures, Structural Dynamics and Materials Conference, Mobile, AL, April 1989, pp. 1832 - 1839.

6 Boyce, L., Keating, J., Lovelace, T. and Bast, C., "Probabilistic Lifetime Strength of Aerospace Materials Via Computational Simulation," NASA CR 187178, NASA Lewis Research Center, Cleveland, Ohio, Aug. 1991.

7 Brinkman, C.R. and Korth, G.E., "Strain Fatigue and Tensile Behavior of Inconel 718 from Room Temperature to 650 °C," Journal of Testing and Evaluation, JTEVA, Vol. 2, No. 4, July, 1974, pp. 249-259.

8 Chamis, C. C., "Simplified Composite Micromechanics Equations for Strength, Fracture Toughness, Impact Resistance and Environmental Effects," NASA TM 83696, Jan. 1984.

9 Chamis, C. C. and Hopkins, D., "Thermoviscoplastic Nonlinear Constitutive Relationships for Structural Analysis of High Temperature Metal Matrix Composites," NASA TM 87291, Nov. 1985.

REFERENCES (continued)

10 Collins, J. A., Failure of Materials in Mechanical Design, Wiley-Interscience Publication, John Wiley & Sons, N.Y., 1981, pp. 391 - 393.

11 Cullen, T. M. and Freeman, J. W., "The Mechanical Properties of INCONEL 718 Sheet Alloy at 800°F 1000°F and 1200°F," NASA CR 268, NASA, Washington, DC, 1985, pp. 20-34.

12 Flinn, R. A. and Trojan, P. K., Engineering Materials and Their Applications, Houghton Mifflin Co., Dallas, TX, 1990.

13 Hopkins, D. A., "Nonlinear Analysis for High-Temperature Multilayered Fiber Composite Structures," NASA TM 83754, Aug. 1984.

14 Hopkins, D. and Chamis, C. C., "A Unique Set of Micromechanics Equations for High Temperature Metal Matrix Composites," NASA TM 87154, Nov. 1985.

15 INCONEL Alloy 718, Inco Alloys International, Inc., Huntington, WV, 1986, pp. 8-13.

16 Korth, G. E., "Mechanical Properties Test Data of Alloy 718 for Liquid Metal Fast Breeder Reactor Applications," EG&G Report No. EGG-2229, January, 1983.

17 Kuwabara, K., Nitta, A. and Kitamura, T., "Thermal-Mechanical Fatigue Life Prediction in High-Temperature Component Materials for Power Plant," Proceedings of the Advances in Life Prediction Methods Conference, ASME, Albany, N. Y., April, 1983, pp. 131-141.

18 Mendenhall, W., Introduction to Probability and Statistics, Duxbury Press, North Scituate, Massachusetts, 1979, p. 48.

19 Ross, S. M., Introduction to Probability and Statistics for Engineers and Scientists, Wiley, New York, 1987, p. 278.

REFERENCES (continued)

20 Scott, D. W., "Nonparametric Probability Density Estimation by Optimization Theoretic Techniques," NASA CR-147763, April 1976.

21 Shigley, J. E. and Mischke C. R., Mechanical Engineering Design, 5th Ed., McGraw-Hill, N. Y., 1989, p. 161.

22 Siddall, J. N., Probabilistic Engineering Design, Marcel Dekker, Inc., New York, 1983.

23 Sims, C. T., Stoloff, N.S. and Hagel, W.C., Superalloys II, Wiley, New York, 1987, pp. 581-585, 590-595.

24 Swindeman, R. W. and Douglas, D.A., "The Failure of Structural Metals Subjected to Strain-Cycling Conditions," Journal of Basic Engineering, ASME Transactions, 81, Series D, 1959, pp. 203 -212.